UCRL-10673

University of California

Ernest O. Lawrence Radiation Laboratory

MASS-SPECTROMETRIC STUDY OF FISSION FROM THE U^{236} COMPOUND NUCLEUS AT MODERATE EXCITATIONS

DISCLAIMER

UCRL-10673

Research and Development

UNIVERSITY OF CALIFORNIA

Lawrence Radiation Laboratory
Berkeley, California

Contract No. W-7405-eng-48

MASS-SPECTROMETRIC STUDY OF FISSION FROM THE U^{236} COMPOUND NUCLEUS AT MODERATE EXCITATIONS

James Anthony McHugh, Jr.

(Thesis)

February 12, 1963

Printed in USA. Price $2.00. Available from the
Office of Technical Services
U. S. Department of Commerce
Washington 25, D.C.

MASS-SPECTROMETRIC STUDY OF FISSION FROM THE U^{236} COMPOUND NUCLEUS AT MODERATE EXCITATIONS

Contents

MASS-SPECTROMETRIC STUDY OF FISSION FROM THE U^{236} COMPOUND NUCLEUS AT MODERATE EXCITATIONS

James Anthony McHugh, Jr.

Lawrence Radiation Laboratory and Department of Chemistry
University of California
Berkeley, California

February 12, 1963

ABSTRACT

The helium-ion-induced fission of Th^{232} (U^{236*}) has been investigated by using high-sensitivity mass-spectrometric techniques. The nuclear-charge-distribution function was measured directly for one isobaric sequence and indirectly in another; it was found to be Gaussian and independent of the excitation in U^{236*}. An empirical Z_p function was derived from 12 measured fractional independent yields, and compared with the Z_p function from $U^{235}(n_{th},F)$. The various postulates of nuclear charge division were discussed. The total number of neutrons emitted per fission as a function of mass ratio was determined from the Z_p function, the neutron yields being found to depend strongly on the asymmetry of the fission mode.

The relative cumulative yields for the majority of isotopes in the mass 131 to 154 range have been determined. The xenon cumulative yields show no structure at these excitations. Information concerning the distribution of independent yields within an element and the formation of the Kr^{85} isomeric states has been obtained for the helium-ion-induced fission of Th^{232} and U^{235}.

I. INTRODUCTION

Since its discovery, the phenomenon of nuclear fission has been investigated by a variety of methods and techniques. One of the basic methods which contributed greatly to the elucidation of the main features of the fission process is the measurement of fission product yields. Two types of yields are measured, independent and cumulative. An independent yield is one that is not formed by beta decay because the isobaric nuclide of the next lower Z is stable or long-lived, and thus represents a primary product yield after prompt-neutron emission. Yields of this type give information on the division of nuclear charge between the primary fragments. Cumulative yields, on the other hand, result from the beta decay of lower Z members of the fission product chain. Mass distributions are obtained from measurements of this type. A number of excellent review articles summarize these and other aspects of nuclear fission.[1-4]

One of the major advancements in fission-yield measurements occurred when mass-spectrometric techniques were introduced. Thode and Graham[5] were the first to utilize this method, and applied it to the measurement of Kr and Xe yields produced from the thermal-neutron fission of U^{235}. In the ensuing years, practically all the major cumulative yield products produced in slow-neutron fission have been investigated in the mass spectrometer.[6-24] This technique has not been extensively applied to charged-particle induced fission mainly because of the low product yields ($< 10^{-9}$ g). Chu and Michel,[21] however, showed that with high-sensitivity mass spectrometry and careful chemistry, the relative abundances of a number of elements from charged-particle fission could be determined. Two advantages possessed by mass spectrometry as compared with radiochemistry are readily apparent: (a) Stable-isotope yields can be measured in addition to radioactive species (this is a distinct advantage especially in the measurement of cumulative yields, and of independent yields produced in fission from moderately excited nuclei). (b) In addition to the high precision of this technique, the accuracy compared to radiochemical methods is enhanced because of the elimination of the usual radiochemical problems

(decay-curve resolution, knowledge of the decay scheme, and counting efficiencies).

A large body of data has been obtained relating to the mass and charge distributions in $U^{235}(n_{th},F)$.[23-26] However, detailed studies of the energy dependence of various fission features (especially charge distribution) through a wide range of excitation in U^{236*} are scare. Radiochemical studies of the helium-ion-induced fission of Th^{232} (U^{236*}) were first performed by Newton (in 1949) who observed the competition between the symmetric and asymmetric modes in fission.[27] Later Foreman[28] (1958) and Davis[29](1963) contributed yield results dealing with the mass distribution, and to a lesser extent with charge distribution.

The object of our work was to employ the techniques of high-sensitivity mass spectrometry for the accurate measurement of fission yields resulting from $Th^{232}(He^{4},F)$. In particular, major attention was devoted to independent yield measurements so that a detailed analysis of charge distribution could be made. The comparison of experimentally predicted primary yields with a number of postulates[16,17,26,30-36] concerning nuclear charge division is the general technique for determining the validity of these postulates or prescriptions. However, any interpretation based on experimentally derived primary yields is strongly dependent upon a knowledge of fragment neutron yields. For charged-particle-induced fission, the fragment neutron yields are not known, and thus any ambiguity in the neutron yield will be reflected in the predicted primary yield. Therefore, these experimentally derived yields will not satisfactorily test a proposed mechanism of fission charge distribution. As an alternative, we have taken our primary yield information and directly extracted information concerning neutron yields as a function of mass ratio. From an appropriate charge division mechanism, fragment neutron yields can be predicted.

In addition to the helium-ion-induced fission of Th^{232}, the relative rare-gas yields were measured for $U^{235}(He^{4},F)$ and $U^{235}(n_{th},F)$. The results for neutron fission of U^{235} were a repeat of earlier works.[12,16]

II. EXPERIMENTAL PROCEDURES

A. Target Preparation and Irradiation

1. Target Materials.

In the bombardments where rare gas, cesium, or rubidium yields were measured, the target material consisted of 0.001-in. thorium metal foils. The foils were cut to the proper target dimensions, then weights and areas of all foils were measured for the purpose of accurately calculating the energy loss of the helium-ion beam. For cyclotron irradiations, it was established that metal foils retain a large representative fraction of the rare-gas fission products. Metal oxide targets, on the other hand, were observed to lose appreciable amounts of fission gases. On one occasion a ThO_2 target yielded erroneous Cs (Xe daughter) ratios that could only be ascribed to a Xe loss. From these results and the correct ratios, a lifetime of 9 min was calculated for Xe in the target under irradiation. Therefore metal foils were used exclusively whenever a measurement of a rare-gas isotope or its daughters was to be made.

In the bombardments where rare-earth fission yields were measured, the target material consisted of purified ThO_2. Purification of the target material is necessary since the stock material contains an amount of a given rare-earth isotope far exceeding the amount made in a single irradiation (which is of the order of 10^{-9} to 10^{-10} g). Natural contamination will completely obscure the fission-produced isotopes if not kept to a minimum.

Elution of Th^{4+} from anion-exchange resin with nitric acid is the basis of the purification process. Thorium adsorbs on anion resin in moderate concentrations of nitric acid; whereas, the rare earths do not adsorb to any great extent.[37] The purification was accomplished by the following procedure: Chemically pure thorium foil was dissolved in concentrated HCl. An equal amount of concentrated HNO_3 was added and the resultant solution evaporated to near dryness. The remaining solution was made 7M in HNO_3 in as small a volume as possible and then was passed through an anion-exchange (Dowex-1) column. The column was washed with 7M HNO_3

for several column volumes, after which the thorium was removed with dilute HCl. The effluent containing the thorium was collected and made 7M in HNO_3, and again was passed through a clean anion-exchange column. Upon completion of the column washings, the thorium was eluted and precipitated as the hydroxide with NH_4OH. The purified hydroxide was transferred to a quartz crucible and ignited to ThO_2.

2. Irradiation.

A conventional microtarget or "cat's-eye" target was used for mounting the foil targets.[38] Stacked foil targets were employed in most irradiations in order to conserve cyclotron time. A typical bombardment intended for rare-gas analysis required the accumulation of at least 50 to 100 μA-h at a beam intensity of ≈ 8μA. Single foil targets were used in short bombardments whenever fission yield measurements were to be performed quickly (for example, the measurement of the Cs^{136} fractional chain yield). In stacked-foil irradiations, it was not necessary to sandwich the target material between recoil catcher foils. We found that the catcher foils did not contain a significant fraction of the fission events. If the recoils were added to the target foil for analysis, no change in fission product composition would be observed. Therefore catcher foils were not included in our analysis since no absolute cross-section measurements were made.

Due to the physical form of the purified target material (ThO_2), a special type of target was required. The target was made by hydraulically pressing the ThO_2 into a depression in a 1/16-in. copper plate. The plate was constructed to fit a modified microtarget. The depth of the depression (0.0025 to 0.0035 in.) was chosen in such a way as to produce the desired energy loss of the helium-ion beam in the target material.

Front cover foils of 0.001-in. aluminum were used in all irradiations. If a lower-energy bombardment was desired, the helium-ion beam was degraded by weighed aluminum foils placed directly in front of the target. The energy degradation in aluminum and thorium foils was determined from the range energy tables of Williamson and Boujot.[39]

All helium-ion bombardments less than 48-MeV were performed on the Crocker Laboratory 60-inch cyclotron. The Lawrence Radiation Laboratory 88-inch cyclotron was employed for the irradiations above 48 MeV.

B. Solid-Sample Preparation

1. General Target Chemistry

The ultimate sensitivity that can be obtained with the mass spectrometer in the measurement of fission yields is usually limited in practice by natural contamination. If a fission yield of interest is a stable isotope, there exists the possibility that contamination from natural sources can occur. Therefore, the carrier-free target chemistry was made as straightforward as possible: All useless or needless operations in the handling of the sample were eliminated, all implements and vessels used in the sample preparation were scrupulously cleaned, and all reagents required in the chemistry were purified.

a. Reagents. Since the "cleanliness" of the chemistry depends strongly on the purity of the reagents, special care was taken in their preparation. The 7M nitric acid was prepared by redistilling reagent grade (C.P.) HNO_3 from quartz, then collecting the distillate in conductivity water until the desired concentration was reached. Conductivity water was procured by double distilling (from quartz) the effleunt of a mixed-bed ion-exchange column.[40] Hydrochloric acid and ammonium hydroxide were made through the dissolution of their respective anhydrous forms (HCl and NH_3 gases) in conductivity water. The removal of possible-rare-earth contaminates from the lactic acid (the eluting agent used in the rare-earth separations) was accomplished by passage of the lactic acid through a Dowex-50 cation-exchange column. At a low pH, the distribution of rare earth between lactate and resin is greatly in favor of the resin; thus, the rare earths remain on the column.

b. Removal of the target material from fission products. The irradiated Th foils were first cut up for the purpose of removing the excess material that was not activated during the bombardment. The active

3 months to 1 year, thus necessitating a reactivation. In all cases re-bombardment contributed less than 1% to the chains already present and, therefore, any incomplete decay of the newly formed products does not appreciably change the existing fission yields. The elution was monitored by γ - counting all collected fractions. A typical elution curve is shown in Fig. 1. All separations were run under identical conditions in order to eliminate the need for γ -pulse-height analysis (identification) of the various elution peaks in succeeding separations. The peaks other than rare earths found throughout the elution spectrum result from various fission products which also pass through the initial Dowex-1 column. In no case do these interfere with the mass analysis.

The spikes used to interrelate the rare-earth elements were prepared by weighing known amounts of separated isotopes of interest and diluting them to the desired concentrations ($\approx 10^{-12}$ g/μliter).[44]

C. Gas-Sample Preparation

In order to take advantage of the high sensitivity of the mass spectrometer, a sample-preparation system is required that will extract the rare-gas fission products free of undesirable gases—hydrocarbons, O_2, N_2, H_2O, etc.—from the target. Natural contamination of the fission-produced Kr and Xe presents no problem because of their extremely low natural abundances and the ease with which ordinary metallurgical processes remove them from target materials. Hydrocarbon contamination, on the other hand, can be a problem at the sample level at which we are working (10^{10} to 10^{12} atoms). If not eliminated, the heavy-mass hydrocarbons will obscure the fission-produced isotopes. For this reason and to reduce excessive handling, a bakeable gas-preparation and -purification system was constructed and attached directly to the mass spectrometer.

1. Target Melting Assembly

The extraction of the rare gases from the target can be handled either by chemical dissolution or by vacuum fusion. The vacuum fusion technique was chosen because of its simplicity and cleanliness. The

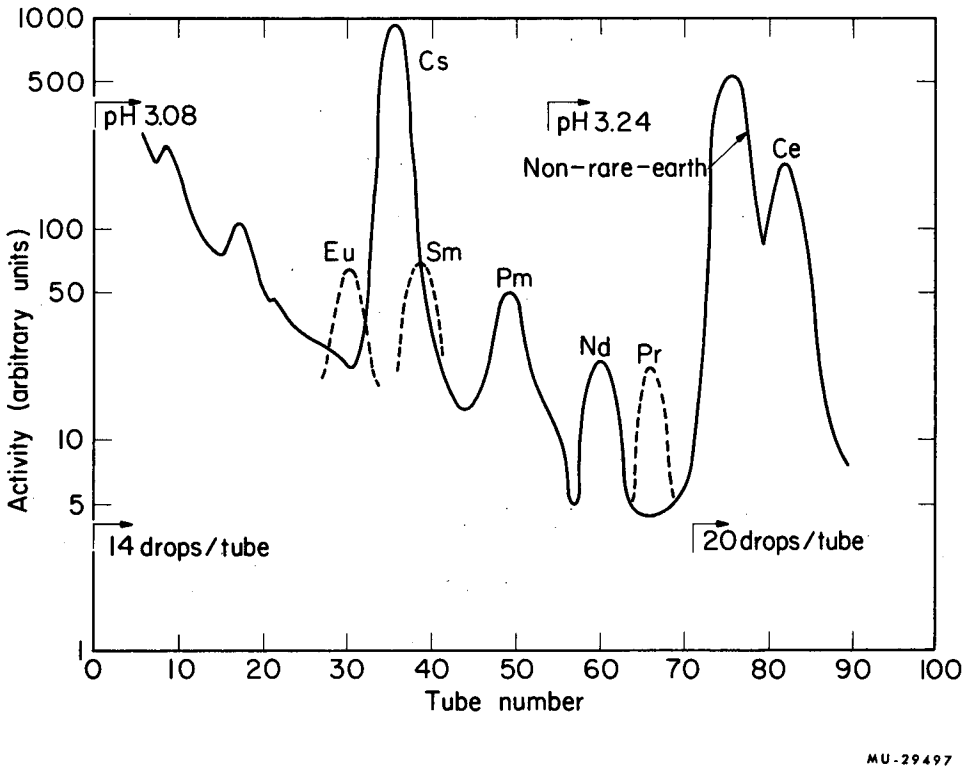

Fig. 1. Elution curve for the light rare-earth elements. Dashed curves represent interpolated positions from rare-earth systematics and column calibration.

fusion was performed by electrical-resistance heating of the target container (tungsten boat). The target container or tungsten boat is formed by folding lengthwise a 3/4- by 4-in. strip of 0.001-in. tungsten foil. The boat is supported between stainless steel jaws attached to the lead-in electrodes (see Fig. 2.). The electrode leads are brought in through Advac insulators[45] that are welded to a stainless steel plate. The electrode assembly is sealed to the stainless steel vacuum chamber by a copper gasket-knife edge seal. The seal is bakeable and readily demountable for sample introduction. A tantalum radiation shield was placed around the electrode-boat assembly to conserve power and to confine the spread of radioactivity within the chamber. The tungsten boat containing the target of interest was heated by direct passage of current from a step-down transformer capable of supplying 200 A at 15 V rms.

2. Purification System

The apparatus designed and constructed for the rare-gas purification is shown diagrammatically in Fig. 3 and is pictured in Fig. 4. It consisted of three major sections: the melting chamber (already described), the charcoal trap, and the getter. (A getter is a material which is included within a vacuum system or vacuum tube for sorption of residual gases and vapors). The apparatus was assembled of 3/8-in. stainless steel tubing and a small portion of 10-mm pyrex tubing. The packless all-metal isolation valves (bakable-diaphragm type) used throughout the system were commercially available.[46] The bakeable inlet valve to the mass spectrometer was patterned after the design of Alpert.[47] A demountable oven completely enclosed the gas-handling system.

The gettering action of hot titanium metal was used to remove the unwanted gases released in the melting operation.[48] Strips of 0.002-in. Ti foil 1-3/8 in. wide were corrugated and coiled to form a cylindrical element 2 in. in diameter. Two such elements were contained within a welded 2- by 4-in. stainless steel container attached to the preparation line. A furnace capable of heating the getter to at least 850°C was constructed from tube furnace heater elements of 2-3/8-in. i.d.

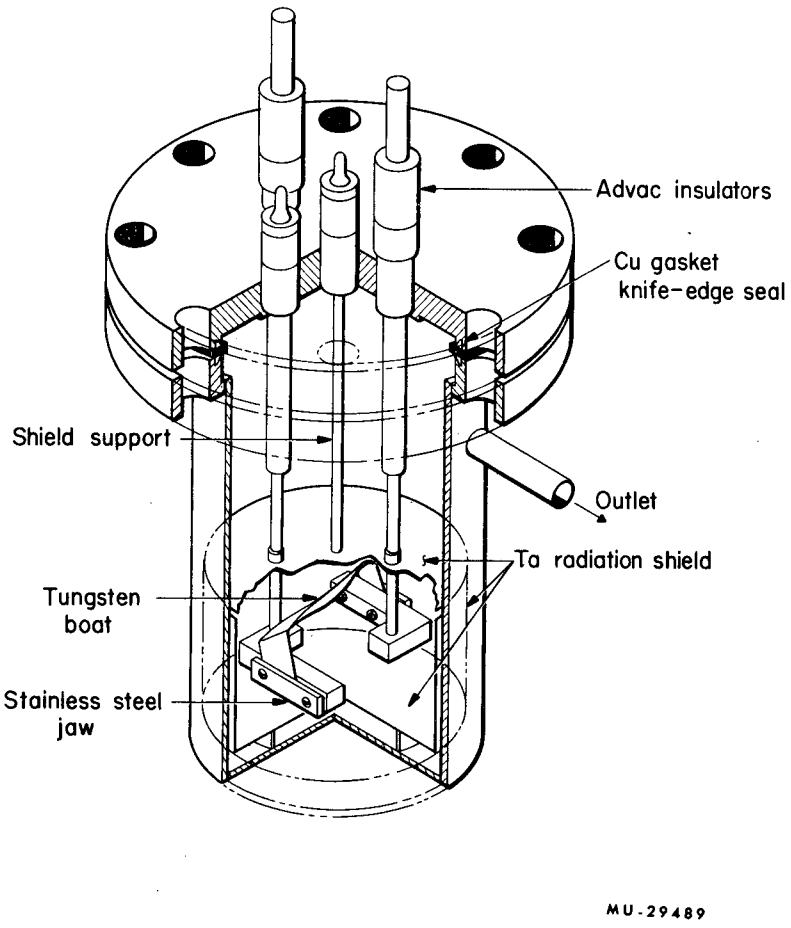

Fig. 2. Target melting chamber.

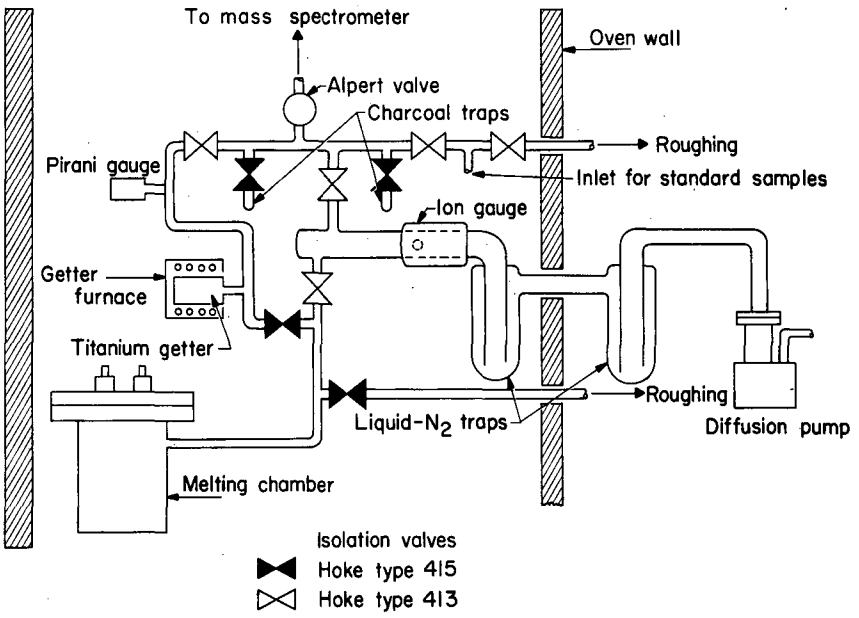

Fig. 3. Schematic diagram of the rare-gas handling and purification system.

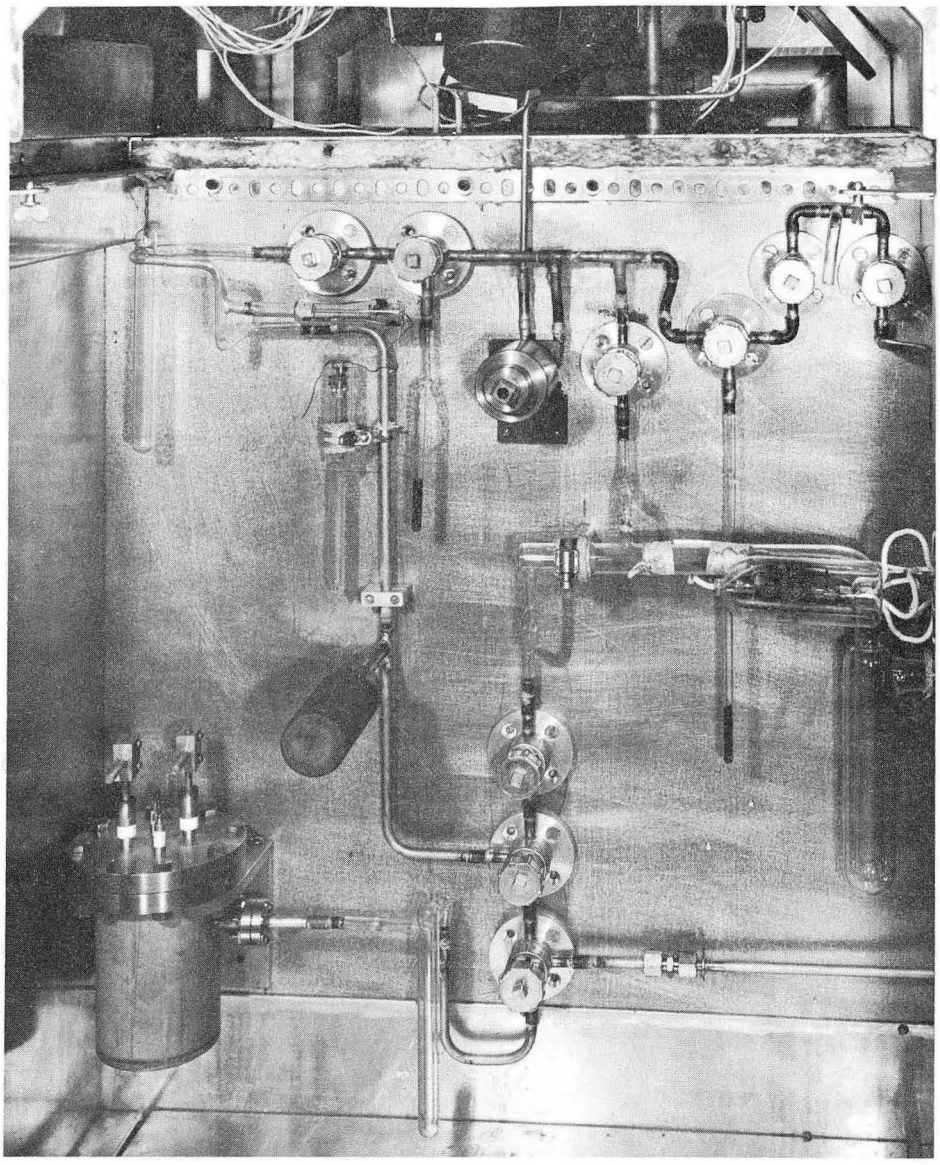

ZN-3592

Fig. 4. Rare-gas handling and purification system.

A Sylvania (R1111M) Pirani gauge was placed in the system to monitor the gas pressure during the melting operation and to monitor the gettering action of the hot titanium. An ion gauge was excluded from the preparation line because of its pumping action.

In order to concentrate the purified Kr and Xe fission products, a charcoal trap was placed adjacent to the mass-spectrometer inlet valve. The Kr and Xe are condensed at liquid-nitrogen temperature on the charcoal, then are isolated from the remainder of the preparation system and are expanded into the mass spectrometer.

The vacuum system associated with the sample-preparation system is composed of a 5-liter oil (octoil-S) diffusion pump preceded by two liquid-nitrogen traps in series (trap closest to system is bakeable). Multiple trapping was introduced to reduce hydrocarbon back-streaming. However, in our operation one trap was found to be sufficient.

3. Preparation Procedure

The gas sample preparation procedure was as follows: A foil target which had "cooled" for a predetermined time was placed within a newly formed tungsten boat clamped to the electrode assembly. The boat was replaced after each melting because cross contamination could occur if a portion of the previous sample remained unmelted, and because the boat is physically weakened by reaction with the target material and by recrystallization. The melting chamber was sealed, and the whole preparation system given a complete bakeout.

For succeeding samples it was unnecessary to bake the entire preparation line since the melting chamber could be isolated from the remainder of the system and was thus the only portion exposed to the atmosphere. However, the titanium getter and the charcoal trap, because of their large surface areas, were individually baked out at 400°C prior to each analysis to ensure against cross contamination. Upon completion of the bakeout, the sample preparation line was isolated from the diffusion pump. The target (Th or U) was melted by passing a large current through the tungsten target container. Normally all targets melted at or below a current of 90 A in the tungsten boat.

In the meantime the titanium getter was heated to 850°C and maintained at that temperature for approximately 1/2 h. The pressure rise that accompanied the melting never exceeded 50 μ Hg, and after gettering, the pressure was well below the detection limit of the Pirani gauge.

It should be noted that the target materials (Th and U) also posess chemisorption properties at elevated temperatures. When the getter had cooled to room temperature, the purified rare-gas fission products were pumped to the liquid-nitrogen cooled charcoal trap, isolated from the getter and melting chamber, and expanded into the mass spectrometer in preparation for static analysis.

D. Mass Spectrometers

1. Solids Mass Spectrometer

The solid sample analyses were performed with a 12-in.-radius 60-deg-sector single-direction-focusing mass spectrometer of symmetrical design. A double-filament surface-ionization source was used to generate the 10-kV positive-ion beam. The metal oxides of the sample were evaporated from a tungsten filament and ionized at a higher temperature rhenium filament. A secondary electron multiplier of the Allen design[49] was used to detect the resolved ion beam. The output of the electron multiplier was either integrated and amplified by a vibrating-reed electrometer, or ion-counted by using a fast pulse-counting system.[50] To focus the isotopes of interest, magnetic scanning was employed when the multiplier output was integrated; whereas, voltage scanning (stepping) was used if the output was ion-counted. Additional features of the mass spectrometer include a Stevens-type vacuum lock[51] which permits rapid introduction of samples, a pumping system capable of maintaining a 2×10^{-8}-torr operating pressure, and a nuclear magnetic resonance fluxmeter for mass calibration.

The mass-spectrometer sensitivity is such that routine measurements can be performed on rare-earth samples of 5×10^{-12} g. Normally our fission product sample size was in the 10^{-9}- to 10^{-10}-g range.

2. Gas Mass Spectrometer

The gas mass spectrometer is a 6-in.-radius 60-deg-sector single-direction-focusing instrument which also employs an electron multiplier detector. The conventional electron-impact ion source is operated at 3 kV ion-accelerating potential with a regulated ionizing current (trap) of 80 μA. A source magnet of 100 G is used to collimate the electron beam. The spectrometer system is constructed of stainless steel and is enclosed by demountable ovens. A liquid-nitrogen-trapped mercury diffusion pump and two 40-liter/sec getter ion pumps compose the spectrometer vacuum system. The mercury diffusion pump is used only in the initial bakeout of the spectrometer. After bakeout, it is isolated from the system by an indium valve;[52] the getter-ion pumps then take over the system pumping. A base pressure of 8×10^{-10} torr, as measured by a modified Bayard-Alpert type ionization gauge, is readily obtained.

Bakeouts at 200°C were found sufficient to reduce the hydrocarbon background in the Kr and Xe mass region to levels below or just above detectability. For example, a xenon isotope exhibiting a partial pressure of $\approx 10^{-15}$ torr in the mass spectrometer is detectable. Xenon measurements for cyclotron targets were performed with ion beam intensities that were a factor of $\approx 10^{5}$ above the detectable limit.

All samples were analyzed under static conditions. That is, the fission product gas samples were introduced to the mass spectrometer after all pumping had been suspended, and then were analyzed. In using the static method of analysis the sample under investigation would become slightly contaminated by a mixture of previous samples. The contamination or memory is released by ion bombardment. It can be controlled so as not to interfere with subsequent measurements through bakeouts and fast analyses; however, it cannot be completely eliminated. This spectrometer memory was also observed by Reynolds.[53]

III. TREATMENT OF DATA

A. Cumulative Yields

For the low- and intermediate-energy fission of a heavy nucleus (e.g., U^{236}), the primary fission products are formed with neutron-to-proton ratios greater than that of the stable nuclei of identical mass. The primary products, therefore, progress up isobaric chains by a series of negatron decays until a long-lived or stable isotope, representing the end product of the fission chain, is reached. The relative yields of the respective fission chains can then be derived from a mass-spectrometric relative-abundance measurement of the chain end products. Fundamentally, this is how the relative chain yields were determined; however, the raw-data treatment requires further discussion because of certain corrections involved.

Despite precautions to prevent stable isotope contamination, slight amounts of natural rare earths were observed in our analyses. The rare-earth column separation eliminates the reaction-produced contamination of adjacent rare earths; therefore, the contamination correction involves only a subtraction of natural relative abundances from the observed fission product relative abundances. The magnitude of the correction is evaluated from the amount of one or more natural isotopes present in the element under investigation. For the element being analyzed, the natural-contamination correction is based on a stable isotope of that element having an insignificant fission yield. Shielded isotopes such as Nd^{142} and Sm^{148} possess both low yields ($\leq$ 1% of chain) and high natural abundances, which together make for accurate subtraction of the natural contamination. In addition to natural contamination by the element under consideration, there was in some instances contamination by neighboring rare-earth elements. Since natural compositions are moderately well known, an accurate correction for these contributions can be made through a relative-abundance measurement of the contaminating element at a mass position not covered by the fission-produced isotopes.

The analyses of the unspiked samples result in a series of partial yield-mass curves due to the different elements. The normalization of

these curves was obtained from the spiked sample. In other words, one atom yield per element was determined from the unspiked and spiked ratios, and from the amount of spike added. In some cases it is possible to normalize the relative yields of adjacent elements through the measurement of a yield they have in common. The mass-144 chain can be measured both in Ce and in Nd since Ce^{144} has an appreciable half-life (285 days), thereby permitting the Ce and Nd relative yields to be normalized without isotope dilution. The Ba^{138} cumulative yield was related to the Cs yields in this manner by measurement of Cs^{136} yield both in Cs and in Ba.

In addition to the rare-earth measurements, relative chain yields were obtained for Kr, Xe, Cs and Ba isotopes. The Xe and Cs yields could be normalized by measurement of the 133 chain yield in both Xe and Cs; however, this was not done here, since all of our targets were allowed to "cool" for a period long compared with the 5-day Xe^{133}. The Cs and Xe yields were normalized by assuming that the Cs^{133} and Cs^{135} yields were consistent with the curve for the Xe yields. We can justify this normalization on the assumption that higher excitation fission has a smoothing effect on possible structure in the yields. This is in agreement with our rare-earth results in that the graphically normalized partial curves agree with the isotopic dilution normalization within the spiking accuracy.

A yield-mass curve was obtained for the 131- to 154- mass region by normalizing our 131 to 138 and 142 to 154 curves through the use of radiochemical yields.[28,29] A rare-earth cross section was chosen from the best fit of the radiochemical yield-mass results to our rare-earth curve, and used along with a similarly obtained cross section from the Xe region as a basis for normalization. The accuracy of such a normalization is not expected to be as high as the mass-spectrometric precision ($\approx 1\%$) of the relative yields; however, it is hoped to be better than 10% since we used several radiochemical cross sections which best fit our accurate relative yields.

In some instances, the measured yield did not represent the total chain yield. The remainder of the chain is located in isotopes of higher Z. To obtain the correct yield, one could measure and add yields of the higher-Z isotopes, or apply a correction to the partial yield based on the charge distribution in that isobaric sequence. Both methods

were employed; for example, the Sm^{150} and Nd^{150} yields were summed to obtain the 150 total chain yield; whereas, the Cs^{137} cumulative yield (a cumulative yield represents the sum of all independent yields preceding and including the given isotope) was corrected by using our charge distribution curve and estimating the fraction of the chain beyond Cs.

B. Independent Yields

1. Shielded Isotopes

The yields of isotopes that are shielded by stable or long-lived isotopes from their β^- decay chains represent independently formed fission products. Shielded-isotope measurements comprise most of the unambiguous results on independent fission yields, but since these isotopes lie so close to β stability, lower-energy fission measurements were hampered by their extremely low yields. It is possible at higher excitations to make accurate mass-spectrometric measurements on these shielded isotopes which would then contain an appreciable fraction of the total chain yield. The fraction of the total chain yield formed independently is of extreme importance in interpreting or attempting to interpret nuclear charge division in fission (which is discussed in a later section).

The Cs^{136}, Cs^{134} and Cs^{132} independent yields were measured relative to the Cs^{137} chain yield. From the previously determined relative chain yields of Xe and Cs, one can obtain fractional chain yields for these isotopes. The independent yields of I^{130}, I^{128}, and I^{126} were obtained through measurement of their stable daughters—Xe^{130}, Xe^{128} and Xe^{126}—relative to the Xe^{131} chain yield. The contribution of the daughter to the yield is in most cases very small, and an accurate correction can be made by using our charge distribution function. The yield of Xe^{129} that is shielded by the 10^7-year I^{129} was also measured in the same run. Fractional chain yields for these isotopes, likewise, result from a knowledge of the relative chain yields in this region. However in this case we must extrapolate our relative yield-mass curve to lighter mass (126).

This was accomplished by a smooth extrapolation based on analysis of radiochemical data in this region.[28,29] The accuracy of such an extrapolation is expected to be better than 5%. The independent yields of Br^{82} and Br^{80} were measured in their Kr daughters relative to the Kr^{84} chain. The necessary relative chain yields for the 82 and 80 chains were derived from an extrapolation of our Kr chain measurements based on a reflection of the complimentary rare-earth relative yields. The Br^{80}, I^{126}, and I^{128} exhibit branched decay between β^+, electron capture, and β^- modes. Branching ratios from Strominger et al.[54] were used to correct the observed yields. The Pm^{150} fractional chain yield was measured in its stable daughter, Sm^{150}.

The independent yield of Rb^{86} was measured. However, in this measurement natural Rb contributed appreciably to the mass-85 and mass-87 fission yields. In order to obtain the yield of Rb^{86} relative to the Rb^{87} chain yield, an assumption concerning magnitude of natural contamination had to be made. Since Rb^{85} is the major natural isotope and is a partial chain yield ($\approx$ 70%) because of hold-up in Kr^{85}, it was assumed to be all natural. This results in an error such that the Rb^{86} fractional chain yield is an upper limit. The relative chain yields at these mass positions were determined by a method identical to that in the previous bromine discussion.

2. Decay Equation for the Mass-135 Chain

In order to obtain direct information concerning the charge-distribution shape, fractional chain yields for two or more members of a fission product chain are required. By observing the growth rate of the long-lived Cs^{135} from the isobaric chain, it is possible to calculate from the equations of radioactive transformation, the major primary yields in this chain. The fractional yields of Cs^{135} and Xe^{135}, and fractional cumulative yield of I^{135} have been measured by this method.

The observation of the growth was made by chemically separating the Cs^{135} from its precursors at a specified time, then measuring the accumulated Cs^{135} relative to Cs^{137} (Cs^{137} precursors have completely decayed prior to Cs separations). Observations were performed for three decay times: approximately 1 h, 13 h, and 8 days after irradiation.

Upon consideration of the 135 decay chain,[24,54] where x, y, and z

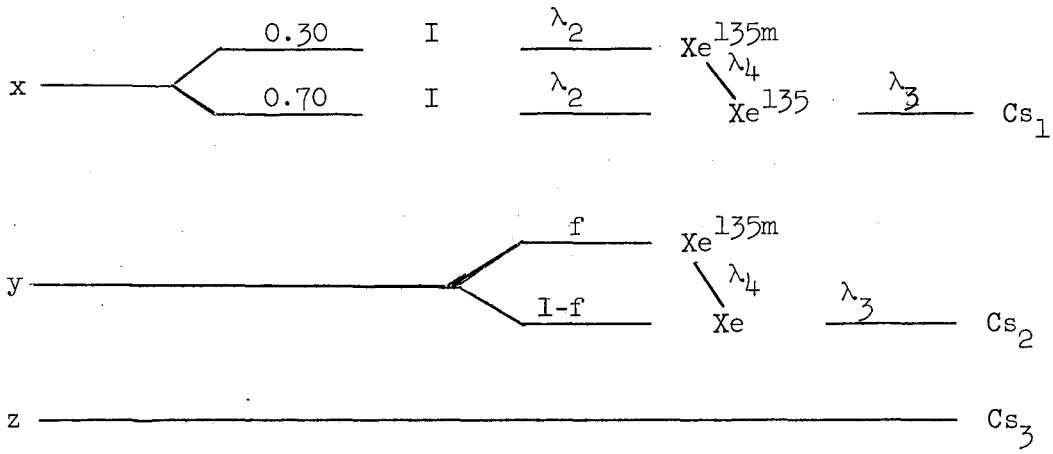

are the independent production rates of I, Xe, and Cs respectively, and f is the fraction of the independent yield which populates the 15-min Xe^{135} isomer, we can derive an expression for the observed Cs^{135} yields as a function of the production rates, time from beginning of irradiation to separation, t, and the length of irradiation, T. See sketch and Eqs. (1), (2), and (3).

$$Cs_1 = 0.7\,x \left\{ T - \frac{\lambda_2 \exp(-\lambda_3 t)}{\lambda_3(\lambda_2 - \lambda_3)}[\exp(\lambda_3 T)-1] + \frac{\lambda_3 \exp(-\lambda_2 t)}{\lambda_2(\lambda_2 - \lambda_3)}[\exp(\lambda_2 T)-1] \right\}$$

$$+ \; 0.3x \left\{ T - \frac{\lambda_2\lambda_3 \exp(-\lambda_4 t)}{\lambda_4(\lambda_2 - \lambda_4)(\lambda_3 - \lambda_4)} [\exp(\lambda_4 T)-1] \right.$$

$$- \frac{\lambda_4\lambda_3 \exp(-\lambda_2 t)}{\lambda_2(\lambda_2 - \lambda_4)(\lambda_2 - \lambda_3)} [\exp(\lambda_2 T)-1]$$

$$\left. + \frac{\lambda_2\lambda_4 \exp(-\lambda_3 t)}{\lambda_3(\lambda_2 - \lambda_3)(\lambda_3 - \lambda_4)} [\exp(\lambda_3 T)-1] \right\}, \qquad (1)$$

$$Cs_2 = fy\left\{T - \frac{\exp(-\lambda_3 t)}{\lambda_3}[\exp(\lambda_3 T)-1]\right\}$$

$$+ (1-f)y\left\{T - \frac{\lambda_4\exp(-\lambda_3 t)}{\lambda_3(\lambda_4 - \lambda_3)}[\exp(\lambda_3 T)-1] + \frac{\lambda_3\exp(-\lambda_4 t)}{\lambda_4(\lambda_4 - \lambda_3)}[\exp(\lambda_4 T)-1]\right\}, \quad (2)$$

$$Cs_3 = zT. \quad (3)$$

Since

$$\frac{Cs^{135}(t)}{Cs^{137}} \propto \frac{Cs_1(x,t,T) + Cs_2(y,t,T) + Cs_3(z,t,T)}{T},$$

three measurements of Cs^{135}/Cs^{137} for t_1, t_2 and t_3 completely specify the production rates x, y, and z, which are directly related to fractional chain yields. The Cs^{135} fractional chain yield is given by $x/(x+y+z)$; similar expressions give the fractional yields of Xe^{135} and I^{135}. If the Ba^{135} fractional chain yield is appreciable, it must be considered. In other words, the above fractional-chain-yield expressions must be multiplied by the fraction of the total chain present. In our measurements the Ba^{135} yield was negligible.

IV. RESULTS

A. Cumulative Yields

Table I shows the relative cumulative yields of Ce, Nd, and Sm isotopes for the fission of $U^{236*}(Th^{232} + He^{4})$ at 39.3-MeV excitation. The observed relative yields of each element have been listed separately. These observed yields have been corrected wherever necessary for decay of the isotope under consideration, or for incomplete decay of a precursor by using the first choice of half-lives given by Strominger et al.[54] The yields have been normalized to the mass-143 yield (taken as unity) by methods previously described, and listed in the last column of Table I.

For convenience, we have presented all $Th^{232} + He^{4}(U^{236*})$ results in terms of the excitation of the U^{236*} compound nucleus. Comparisons of results from neutron-induced fission of U^{235} (U^{236*}) and the He^{4}-induced fission of Th^{232} are thus based on the excitation in the U^{236*} system. The He^{4} bombarding energy required to produce a particular U^{236*} excitation E^{*} (MeV) is given by $E_{He^{4}}$ (MeV) $\approx E^{*} + 5.0$ within the energy range used in these experiments.

The relative cumulative yields of Kr, Sr, Xe, Cs, and Ba isotopes are tabulated in Table II. The Kr^{85} yield in the "observed column" represents only the yield of the 10-yr isomer since the shorter-lived 4-h isomer had completely decayed before the fission gases were extracted and analyzed. The Kr and Xe yields were normalized from a knowledge of the relative sensitivity of the mass spectrometer for these isotopes. The sensitivity was determined from an analysis of the rare-gas fraction from thermal-neutron fission of U^{235} where the relative fission yields of Kr and Xe are accurately known.[23]

Tables III, IV, and V contain the relative cumulative yields of Kr, Xe, and Cs for a number of U^{236*} excitation energies. The relative cumulative yields of Kr and Xe for the He^{4}-induced fission of U^{235} are listed in Table VI. All corrections for residual yields in the higher-Z members of an isobaric sequence have been based on the Gaussian charge distribution measured in this work.

Table I. Relative cumulative yields of Ce, Nd, and Sm isotopes in U^{236*} fission at 39.3-MeV excitation.

Mass No.	Observed relative yields			Normalized relative yields
	Ce	Nd	Sm	
142	1.000			1.115 ± 0.025
143		1.000		1.000 ± 0.006
144	0.740[a]	0.825[a]		0.825 ± 0.016
145		0.713		0.713 ± 0.011
146		0.574		0.574 ± 0.010
147			1.490[a]	0.426 ± 0.002
148		0.355		0.355 ± 0.009
149			1.000	0.286 ± 0.002
150		0.218	0.020	0.224 ± 0.006
151			0.598	0.171 ± 0.005
152			0.441	0.126 ± 0.003
154			0.224	0.064 ± 0.0025

[a]Corrected for decay (see text).

Table II. Relative cumulative yields of Kr, Sr, Xe, Cs, and Ba isotopes in U^{236*} fission at 39.3-MeV excitation.

Mass No.	Observed relative yields			Corrected and normalized[a] relative yields	
	Kr	Sr			
83	0.778			(0.778)	0.256
84	1.000			(1.000)	0.330
85	0.309			(1.215)	0.400[b]
86	1.414			(1.416)	0.467
88		1.00		(1.82)	0.600
90		1.24		(2.25)	0.742
	Xe	Cs	Ba		
131	1.000				1.000
132	1.021				1.022
133		1.006			1.033
134	1.012				1.043
135		1.000			1.033
136	0.767		1.00[c]		1.010
137		0.812			0.862
138			3.14		0.764

[a]Corrected for yields in the higher-Z members of the same chain; column in parentheses is the normalized Kr and Sr data, whereas the last column contains the yields of all elements listed relative to Xe^{131}.

[b]Relative mass yield for the 85 chain obtained from a smooth curve fitted to the 83-, 84-, and 86-mass yields.

[c]The Ba^{136} yield contains only independent yields of Cs^{136} and Ba^{136} since it is shielded by Xe. The measured yield represents 0.241 of the total 136 chain yield (determined from measured fractional chain yield of Cs^{136}).

Table III. Relative cumulative yields of Kr and Xe isotopes in U^{236*} fission.

Mass No.	57.0-MeV excitation Relative yields Observed	57.0-MeV excitation Relative yields Corrected[a]	43.5-MeV excitation Relative yields Observed	43.5-MeV excitation Relative yields Corrected[a]
		Krypton		
83	0.800	0.800	0.788	0.788
84	1.000	1.000	1.000	1.000
85	0.343	1.190[b]	0.312	1.200[b]
86	1.338	1.361	1.376	1.384
		Xenon		
131	1.000	1.003	1.000	1.000
132	0.970	0.981	0.993	0.998
134	0.833	0.925	0.957	1.007
136	0.465	0.830	0.670	0.957

[a]Corrected for yields in the higher-Z members of the same chain.

[b]Relative mass yield for the 85 chain, obtained from a smooth curve fitted to the 83, 84, and 86 mass yields.

Table IV. Relative cumulative yields of Kr and Xe isotopes in U^{236*} fission.

Mass No.	37.1-MeV excitation		35.1-MeV excitation		33.1-MeV excitation	
	Relative yields		Relative yields		Relative yields	
	Observed	Corrected[a]	Observed	Corrected[a]	Observed	Corrected[a]
			Kryton			
83	0.772	0.772	0.770	0.770	0.760	0.760
84	1.000	1.000	1.000	1.000	1.000	1.000
85	0.303	1.218[b]	0.295	1.221[b]	0.291	1.229[b]
86	1.416	1.417	1.426	1.426	1.434	1.434
			Xenon			
131	1.000	1.000	1.000	1.000	1.000	1.000
132	1.027	1.027	1.034	1.034	1.046	1.046
134	1.046	1.074	1.049	1.074	1.074	1.095
136	0.819	1.061	0.840	1.063	0.899	1.104

[a]Corrected for yields in the higher-Z members of the same chain.

[b]Relative mass yield for the 85 chain, obtained from a smooth curve fitted to the 83, 84, and 86 mass yields.

Table V. Relative cumulative yields of Kr, Xe, and Cs isotopes in U^{236*} fission.

Mass No.	31.1-MeV excitation Relative yields Observed	31.1-MeV excitation Relative yields Corrected[a]	28.7-MeV excitation Relative yields Observed	28.7-MeV excitation Relative yields Corrected[a]	23.1-MeV excitation Relative yields Observed	23.1-MeV excitation Relative yields Corrected[a]	21.0-MeV excitation Relative yields Observed	21.0-MeV excitation Relative yields Corrected[a]
				Krypton				
83	0.749	0.749	0.737	0.737	0.710	0.710	0.691	0.691
84	1.000	1.000	1.000	1.000	1.000	1.000	1.000	1.000
85	0.291	1.234[b]	0.285	1.243[b]	0.275	1.255[b]	0.269	1.25[b]
86	1.437	1.437	1.445	1.445	1.481	1.481	1.505	1.505
	Xe Cs		Xe Cs		Xe Cs		Xe Cs	
131	1.000	1.000	1.000	1.000	1.000	1.000	1.000	1.000
132	1.057	1.057	1.064	1.064	1.106	1.106	1.136	1.136
134	1.102	1.120	1.120	1.134	1.218	1.220	1.271	1.271
135	1.000	1.140	1.000	1.148	1.000	1.233	1.000	1.264
136	0.963	1.156	0.994	1.161	1.144	1.243	1.216	1.246
137	0.847	0.986	0.856	0.998	0.877	1.084	0.923	1.168

[a] Corrected for yields in the higher Z members of the same chain; the Xe and Cs yields have been normalized (see text) to the 131 chain yield.

[b] Relative mass yield for the 85 chain, obtained from a smooth curve fitted to the 83, 84, and 86 mass yields.

Table VI. Relative cumulative yields of Kr and Xe isotopes for fission of U^{235} induced by 43.6- , 38.0-, 33.8-, and 28-MeV He^4.

Mass No.	43.6 MeV Relative yields		38.0 MeV Relative yields		33.8 MeV Relative yields		28.0 MeV Relative yields	
	Observed	Corrected	Observed	Corrected[a]	Observed	Corrected[a]	Observed	Corrected[a]
				Krypton				
83	0.823	0.823	0.814	0.814	0.806	0.806	0.787	0.787
84	1.000	1.000	1.000	1.000	1.000	1.000	1.000	1.000
85	0.380	1.187[b]	0.361	1.193[b]	0.341	1.201[b]	0.320	1.216[b]
86	1.362	1.394	1.379	1.403	1.401	1.415	1.430	1.436
				Xenon				
131	1.000	1.003	1.000	1.002	1.000	1.001	1.000	1.000
132	0.993	1.010	1.006	1.018	1.012	1.019	1.043	1.046
134	0.804	0.976	0.867	1.020	0.934	1.038	1.052	1.109
136	0.390	0.886	0.453	0.924	0.628	1.163	0.728	1.150

[a] Corrected for yields in the higher Z memebers of the same chain.

[b] Relative mass yield for the 85 chain, obtained from a smooth curve fitted to the 83, 84, and 86 mass yields.

The relative yields of Kr and Xe isotopes for the thermal-neutron fission of U^{235} have also been measured and are tabulated in Table VII along with the results of Wanless and Thode.[12] The yields of Xe^{128} and Xe^{130} represent the independent yields of I^{128} and I^{130}, respectively, since these nuclides are shielded from their β^- chains by tellurium isotopes. The irradiation conditions were chosen so as to minimize neutron capture in the fission products. The U^{235} metal foils used in the above analyses were irradiated in a thermal flux of 3.7×10^{12} n/cm^2 per sec for 3 h. The yield of I^{130} was designated as an upper limit because of the presence of a mass-129 peak of comparable intensity. The mass-129 position could be assigned to natural Xe contamination (no hydrocarbon background was present) and the appropriate correction applied to the mass-130 yield. However, since the origin of the mass-129 peak was in question, it was felt that the total observed mass-130 yield should be taken and designated as an upper limit. No peak was observed at the mass-128 positions in our spectra. The smallest detectable peak that could be observed above the electron multiplier background (under static analysis the 10-y Kr decay produces a detectable signal) was taken as the upper limit to the I^{128} yield.

All errors in the relative cumulative yield measurements are of the order of, or less than, 1% unless otherwise designated. If errors are designated, they are derived from the standard deviation in the results of a large number of mass spectra.

B. Fractional Chain Yields

The fractional chain yields of Cs^{135} and Xe^{135}, and the fractional cumulative yield of I^{135}, are listed in Table VIII for fission at excitation energies of 39.3, 26.8, 23, and $\approx$ 17 MeV in the U^{236*} compound nucleus. The yields of Cs^{135} relative to Cs^{137} for three separate decay periods t,* and the duration T of each irradiation have also been tabulated for each energy in Table VIII. It is from these data and the transformation equations derived earlier that the above listed fractional yields are calculated.

*Decay period measured from beginning of irradiation.

Table VII. Relative yields of Kr and Xe isotopes for thermal-neutron fission of U^{235}.

Mass No.	Wanless and Thode[a]	Observed this work
	Krypton	
83	1.000	1.000
84	1.839	1.858
85	0.538	0.539
86	3.715	3.633
	Xenon	
128	1.2×10^{-5}[b]	$< 1.3 \times 10^{-5}$
130	1.71×10^{-4}[b]	$\leqslant 1.13 \times 10^{-4}$
131	1.000	1.000
132	1.496	1.493
134	2.750	2.735
136	2.207	(2.194) 2.184[c]

[a] See reference 12.

[b] The yields of Xe^{128} and Xe^{130} represent the independent yields of I^{128} and I^{130} as measured by Kennett and Thode.[16]

[c] Corrected for neutron capture produced Xe^{136}; value in parentheses is the uncorrected observed relative yield.

Table VIII. Fractional chain yields of 135 chain for fission of U^{236*}

Observed 135/137	t(h)	T(h)	Cs^{135}	Xe^{135}	I^{135}[a]
		39.3-MeV excitation			
0.1665±0.0031	1.57	0.917			
0.6632±0.0060	13.30	0.917			
1.231 ±0.007	197.	0.917	0.098±0.006	0.523±0.010	0.376±0.009
		26.8-MeV excitation			
0.0795±0.0008	1.78	0.883			
0.5174±0.0022	13.07	0.900			
1.169 ±0.010	300.	0.900	0.032±0.004	0.381±0.009	0.586±0.012
		23.0-MeV excitation			
0.0560±0.0018	1.77	0.65			
0.5347±0.0051	14.73	0.65			
1.140 ±0.007	350.	1.07	0.014±0.004	0.333±0.009	0.653±0.015
		15.0- to 18.0-MeV excitation			
0.0191±0.0025	1.78	0.883			
0.3976±0.0066	13.07	0.900			
1.084 ±0.011	300.	0.900	(< 0.009)	0.22 ±0.010	0.78 ±0.02

[a] I^{135} is a fractional cumulative yield.

Table IX shows the fractional chain yields of a number of shielded isotopes produced from the He^4-induced fission of Th^{232}(U^{236*}) for a variety of excitation energies. The independent yields have been measured relative to a neighboring chain yield in the same element. The column designated "measured as" lists for each isotope the manner in which it was measured, and the cumulative yield to which it was compared. The mass-spectrometrically measured ratios are listed under the "observed yield" heading (Cs^{136}, Rb^{86}, and Cs^{132} yields include small decay corrections). The observed independent yields were converted to fractional chain yields by dividing by the relative total chain yield for that particular mass chain. Because a number of independent yields were measured in stable daughters, corrections for the small independent yields of the daughter had to be applied to the observed fractional chain yields. These corrections were determined from the charge-distribution function measured in this work. In addition, the yields measured in the Br^{80}, I^{126}, and I^{128} daughters required correction for branched decay in the parent. The last column of Table IX lists the corrected fractional chain yields along with an explanation of each correction.

Table X shows fractional chain yields for the He^4-induced fission of U^{235} at 43.6-, 38.0-, 33.8-, and 28.0-MeV He^4. An additional correction is required for these results due to the isotopic composition of the target material. The foils used in the experiments were 93% U^{235} and 7% U^{238}. Corrections for the contribution of He^4-induced fission of U^{238} to the independent and chain yields of U^{235} were based on the data of Chu.[21]

The errors quoted for the fractional yields are the result of the standard deviation in the measured ratios plus any uncertainty in the relative chain yield used in deriving the fractional chain yield.

Table IX. Fractional chain yields for fission of U^{236*}

Independent yield of	Measured as	Observed yield	Fractional chain yield[a]	Corrected fractional chain yield
		57.0-MeV excitation		
Br^{80}	$Kr^{80}:Kr^{84}$	($\leq$0.00096)	($\leq$0.0023)	($\leq$0.0025)[b]
Br^{82}	$Kr^{82}:Kr^{84}$	0.0260	0.0400	0.0400±0.0026
I^{126}	$Xe^{126}:Xe^{131}$	0.00171	0.00155	0.0039±0.0004[c]
I^{128}	$Xe^{128}:Xe^{131}$	0.0638	0.0602	0.0633±0.0013[d,e]
Xe^{129}	$Xe^{129}:Xe^{131}$	0.00849	0.00816	0.0082±0.0004
I^{130}	$Xe^{130}:Xe^{131}$	0.350	0.343	0.315±0.004[e]
		43.5-MeV excitation		
Br^{82}	$Kr^{82}:Kr^{84}$	0.0120	0.0183	0.0183±0.0015
I^{128}	$Xe^{128}:Xe^{131}$	0.0205	0.0205	0.0219±0.0006[d]
Xe^{129}	$Xe^{129}:Xe^{131}$	0.00289	0.00289	0.0029±0.0003
I^{130}	$Xe^{130}:Xe^{131}$	0.187	0.187	0.180±0.004[e]
		39.3-MeV excitation		
Br^{80}	$Kr^{80}:Kr^{84}$	($\leq$0.00026)	($\leq$0.00070)	($\leq$0.00076)[b]
Kr^{81}	$Kr^{81}:Kr^{84}$	($<<$0.00014)	($<<$0.00030)	($<<$0.00030)
Br^{82}	$Kr^{82}:Kr^{84}$	0.00847	0.0137	0.0137±0.0003
Rb^{86}	$Rb^{86}:Rb^{87}$	0.00230	0.00267	0.00267±0.00022
I^{126}	$Xe^{126}:Xe^{131}$	0.000101	0.000124	0.00028±0.00005[c]
I^{128}	$Xe^{128}:Xe^{131}$	0.0138	0.0155	0.0165±0.0005[d]
Xe^{129}	$Xe^{129}:Xe^{131}$	0.00113	0.00122	0.00122±0.00013
I^{130}	$Xe^{130}:Xe^{131}$	0.148	0.153	0.149±0.002[e]
Cs^{132}	$Cs^{132}:Cs^{137}$	0.00164	0.00137	0.00137±0.00011
Cs^{134}	$Cs^{134}:Cs^{137}$	0.0377	0.0302	0.0302±0.0013
Cs^{136}	$Cs^{136}:Cs^{137}$	0.278	0.230	0.230±0.008
Pm^{150}	$Sm^{150}:Sm^{149}$	0.020	0.025	0.025±0.003

Table IX. (cont.)

Independent yield of	Measured as	Observed yield	Fractional chain yield[a]	Corrected fractional chain yield
		37.1-MeV excitation		
Br^{82}	$Kr^{82}:Kr^{84}$	0.0073	0.0120	0.0120±0.0006
I^{126}	$Xe^{126}:Xe^{131}$	0.000065	0.000083	0.00019±0.00006[c]
I^{128}	$Xe^{128}:Xe^{131}$	0.0109	0.0121	0.0129±0.0005[d]
I^{130}	$Xe^{130}:Xe^{131}$	0.129	0.133	0.129±0.002[e]
		35.1-MeV excitation		
Br^{80}	$Kr^{80}:Kr^{84}$	(≤0.00022)	(≤0.00058)	(≤0.00063)[b]
Br^{82}	$Kr^{82}:Kr^{84}$	0.00578	0.00963	0.0096±0.0004
I^{128}	$Xe^{128}:Xe^{131}$	0.00823	0.00968	0.0103±0.0004[d]
Xe^{129}	$Xe^{129}:Xe^{131}$	0.00059	0.00066	0.00066±0.00022
I^{130}	$Xe^{130}:Xe^{131}$	0.112	0.117	0.114±0.002[e]
		33.1-MeV excitation		
Br^{82}	$Kr^{82}:Kr^{84}$	0.00471	0.00805	0.0081±0.0004
I^{126}	$Xe^{126}:Xe^{131}$	(≤0.000036)	(≤0.000047)	(≤0.00011)[c]
I^{128}	$Xe^{128}:Xe^{131}$	0.00633	0.00763	0.0082±0.0004[d]
Xe^{129}	$Xe^{129}:Xe^{131}$	(≤0.00057)	(≤0.00064)	(≤0.00064)
I^{130}	$Xe^{130}:Xe^{131}$	0.0930	0.0979	0.0957±0.0025[e]
		31.1-MeV excitation		
Br^{82}	$Kr^{82}:Kr^{84}$	0.00410	0.00732	0.0073±0.0004
I^{128}	$Xe^{128}:Xe^{131}$	0.00460	0.0058	0.0062±0.0004[d]
I^{130}	$Xe^{130}:Xe^{131}$	0.0773	0.0822	0.0806±0.0019[e]

Table IX. (cont.)

Independent yield of	Measured as	Observed	Fractional chain yield[a]	Corrected fractional chain yield
		28.7-MeV excitation		
Br^{80}	$Kr^{80}:Kr^{84}$	($\leq$0.00015)	($\leq$0.00050)	($\leq$0.00054)
Br^{82}	$Kr^{82}:Kr^{84}$	0.00356	0.00647	0.00647±0.00051
I^{126}	$Xe^{126}:Xe^{131}$	($\leq$0.000017)	($\leq$0.000024)	($\leq$0.000054)[c]
I^{128}	$Xe^{128}:Xe^{131}$	0.00315	0.00420	0.0045±0.0003[d]
I^{130}	$Xe^{130}:Xe^{131}$	0.0624	0.0671	0.0660±0.0018[e]
		26.8-MeV excitation		
Cs^{134}	$Cs^{134}:Cs^{137}$	0.0089	0.0076	0.0076±0.0007
Cs^{136}	$Cs^{136}:Cs^{137}$	0.131	0.111	0.111±0.006
		23.1-MeV excitation		
I^{128}	$Xe^{128}:Xe^{131}$	0.0015	0.0021	0.0023±0.0005[d]
I^{130}	$Xe^{130}:Xe^{131}$	0.0321	0.0357	0.0354±0.0021[e]
Cs^{134}	$Cs^{134}:Cs^{137}$	($\leq$0.0078)	($\leq$0.0068)	($\leq$0.0068)
Cs^{136}	$Cs^{136}:Cs^{137}$	0.0813	0.0713	0.0713±0.0045
		21.0-MeV excitation		
Br^{82}	$Kr^{82}:Kr^{84}$	0.0027	0.0056	0.0056±0.0014
I^{128}	$Xe^{128}:Xe^{131}$	0.0011	0.0018	0.0019±0.0002[d]
I^{130}	$Xe^{130}:Xe^{131}$	0.0235	0.0273	0.0273±0.0030
		15.0- to 18.0-MeV excitation		
Cs^{136}	$Cs^{136}:Cs^{137}$	0.0242	0.0223	0.0223±0.0035

[a]Fractional chain yield is the ratio of the observed independent yield to the total chain yield.

[b]Corrected for branching decay (0.92β^-).

[c]Corrected for branching decay (0.44β^-).

[d]Corrected for branching decay (0.936β^-).

[e]Corrected for independent yield of daughter.

Table X. Fractional chain yields for He^4-induced fission of U^{235}

Independent yield of	Measured as	Observed yield	Fractional chain yield	Corrected fractional chain yield[a]
		43.6-MeV He^4		
Br^{80}	$Kr^{80}:Kr^{84}$	0.00051	0.00106	0.0012±0.0003[b]
Kr^{81}	$Kr^{81}:Kr^{84}$	(<0.000086)	(<0.00015)	(<0.00015)
Br^{82}	$Kr^{82}:Kr^{84}$	0.0342	0.0495	0.0525±0.0015
I^{126}	$Xe^{126}:Xe^{131}$	0.0025	0.0028	0.0067±0.0005[b]
I^{128}	$Xe^{128}:Xe^{131}$	0.0808	0.0842	0.0938±0.0015[b,c]
Xe^{129}	$Xe^{129}:Xe^{131}$	0.0121	0.0124	0.0132±0.0004
I^{130}	$Xe^{130}:Xe^{131}$	0.396	0.400	0.376±0.006[c]
		38.0-MeV He^4		
Br^{80}	$Kr^{80}:Kr^{84}$	(≤0.00031)	(≤0.00068)	(≤0.00074)[b]
Br^{82}	$Kr^{82}:Kr^{84}$	0.0258	0.0385	0.0410±0.0016
I^{126}	$Xe^{126}:Xe^{131}$	0.00146	0.00168	0.0041±0.0004[b]
I^{128}	$Xe^{128}:Xe^{131}$	0.0573	0.0616	0.0689±0.0018[b,c]
Xe^{129}	$Xe^{129}:Xe^{131}$	0.0069	0.0071	0.0075±0.0003
I^{130}	$Xe^{130}:Xe^{131}$	0.326	0.329	0.318±0.006[c]
		33.8-MeV He^4		
Br^{82}	$Kr^{82}:Kr^{84}$	0.0180	0.0277	0.0295±0.0015
I^{126}	$Xe^{126}:Xe^{131}$	0.000664	0.00087	0.0021±0.0002[b]
I^{128}	$Xe^{128}:Xe^{131}$	0.0334	0.0371	0.0421±0.0014[b,c]
Xe^{129}	$Xe^{129}:Xe^{131}$	0.0036	0.0038	0.0039±0.0002
I^{130}	$Xe^{130}:Xe^{131}$	0.249	0.254	0.251±0.006[c]

Table X. (Cont.)

Independent yield of	Measured as	Observed yield	Fractional chain yield	Corrected fractional chain yield[a]
Br^{82}	$Kr^{82}:Kr^{84}$	0.0112	0.0181	0.0192±0.0014
I^{126}	$Xe^{126}:Xe^{131}$	0.00020	0.00029	0.00071±0.00015[b]
I^{128}	$Xe^{128}:Xe^{131}$	0.0151	0.0180	0.0204±0.0008[b]
Xe^{129}	$Xe^{129}:Xe^{131}$	0.00154	0.00171	0.0018±0.0001
I^{130}	$Xe^{130}:Xe^{131}$	0.155	0.162	0.164±0.005[c]

[a]All yields corrected for isotopic composition of the target.

[b]Corrected for branching decay.

[c]Corrected for independent yield of daughter.

V. DISCUSSION

A. Charge Distribution

1. Charge-Distribution Function.

The fractional chain yields for three members of the mass-135 decay chain resulting from the He^4-induced fission of Th^{232} are plotted vs Z in Fig. 5. The maximum in the curve fitted to the fractional yields for each energy fixes the value of Z_p. The Z_p is the value (not necessarily integral) of the most probable nuclear charge among fission products of the same mass number.

All the 135 chain results are presented as a function of $(Z-Z_p)$ in Fig. 6. The fractional yield data are consistent with a Gaussian curve

$$\bar{y}_i = (c\pi)^{-\frac{1}{2}} \exp\left[-(Z-Z_p)^2/c\right],$$

where $\bar{y}_i$ is the fractional independent yield of a chain member having atomic number Z, and c is the normalization or width constant of the distribution. The value of c which best fits all energies is 0.95 ± 0.05.

Wahl et al.[26] have measured fractional yields for two or more members of several decay chains in the thermal-neutron fission of U^{235}. The value of c obtained from a weighted average of the several chains was 0.94 ± 0.15. Since the same compound nucleus (U^{236*}) was produced in both researches, the above results indicate that a single charge-distribution function is maintained through a wide range of excitations (6.5 to 39 MeV). The charge-distribution curve reported by Blann[55] for Au + C^{12} fission is essentially the same as that found here, within experimental error. These results substantiate the previous conclusions, and in addition, suggest that there also exists an independence of the charge dispersion with the mass of the fissioning nucleus. Pate et al.[56] observed an invariance in the dispersion width at lower energies for the proton-induced fission of Th^{232}.

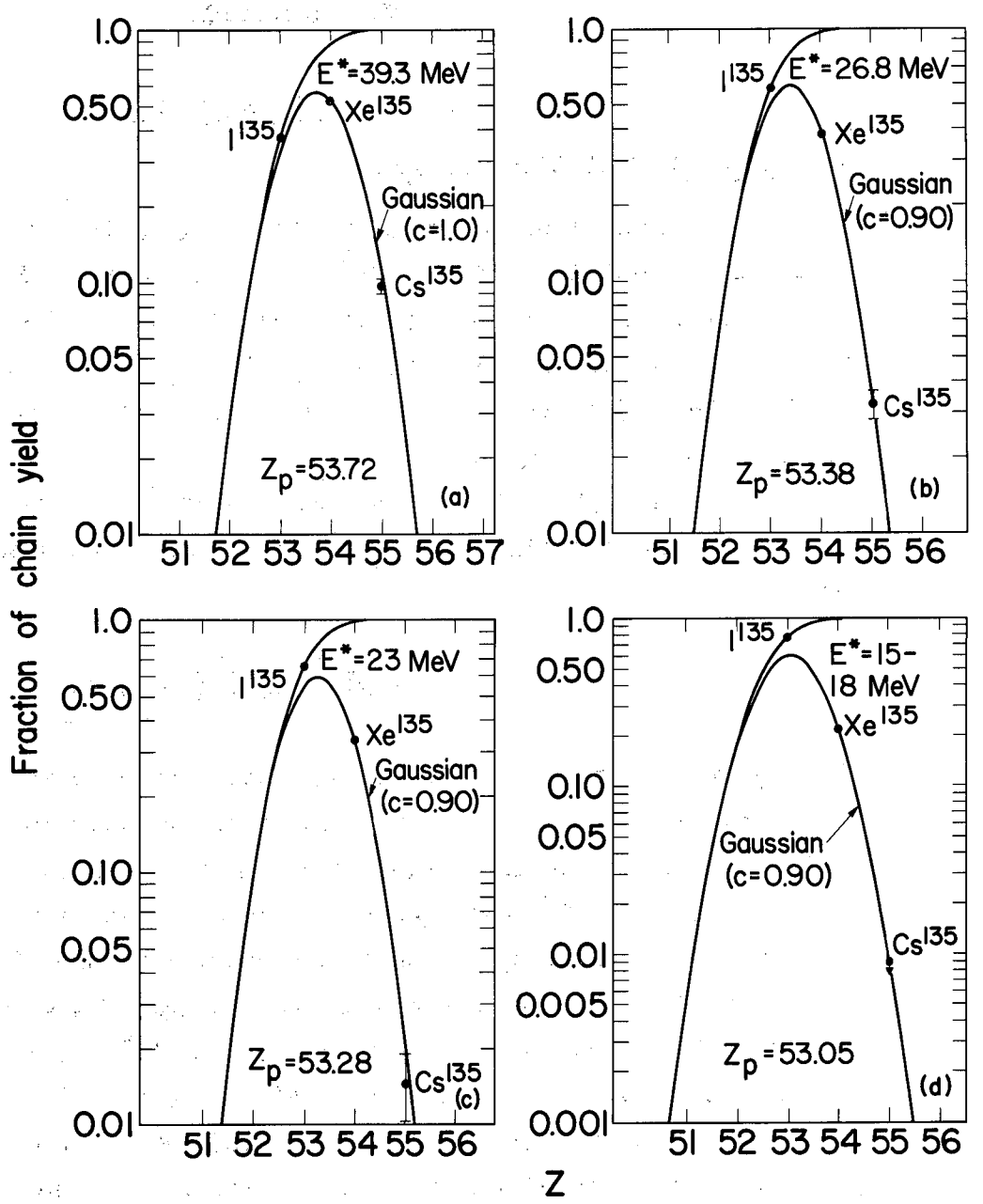

Fig. 5. Gaussian charge-distribution curves fitted to fractional-yield data. The iodine fractional cumulative yields are fitted to an integrated curve based on the Gaussian distribution.

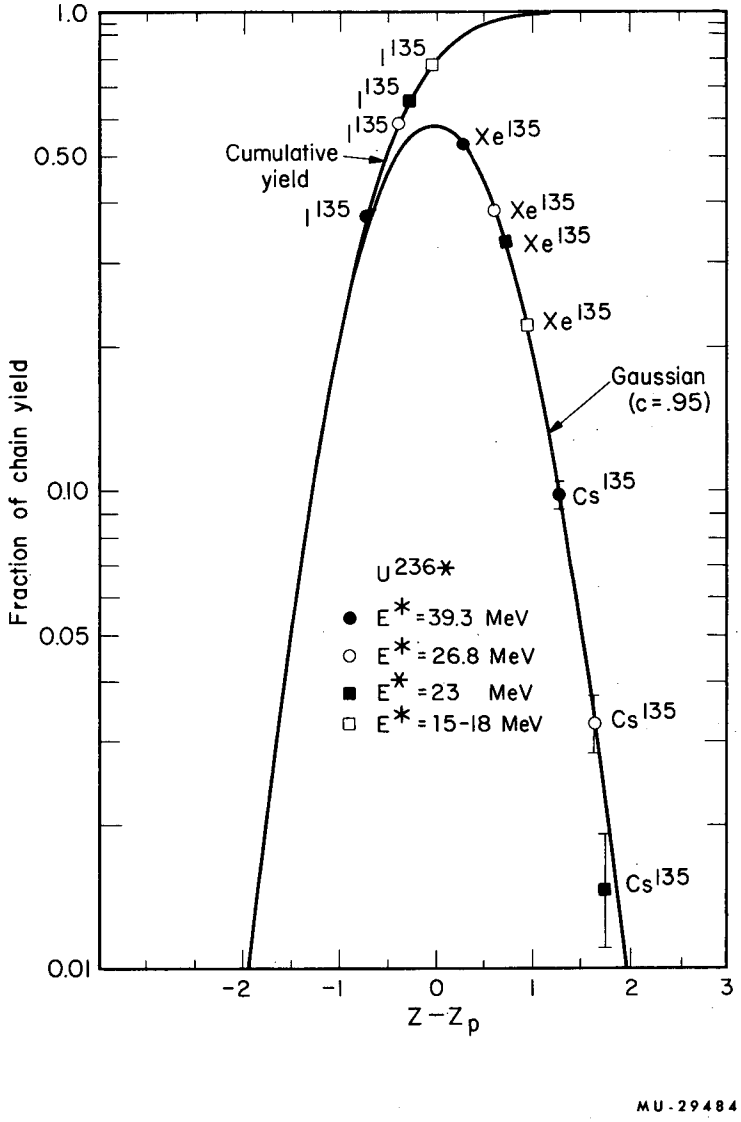

Fig. 6. Gaussian charge-distribution curve which best fit the fractional yield data of the mass-135 chain for all energies.

Swiatecki and Blann[57] have pointed out that a Gaussian charge-distribution function results if the charge fluctuations for a system in thermodynamic equilibrium with harmonic restoring forces can be attributed to statistical and quantum fluctuations. A quantum statistical relationship between the charge-distribution width constant c and the nuclear temperature (related to excitation energy) was derived that is valid for all nuclear temperatures. Their relationship indicates that the width constant should be independent of temperature within the range of excitations that have been reported here (as is observed).

The fractional chain yield of Cs^{136} and the fractional cumulative yield of Xe^{136} for the He^{4}-induced fission of Th^{232} and U^{235} are fitted best with the identical distribution function found for the 135 isobaric sequence. See Fig. 7.

Due to the close proximity of the 82 neutron shell to the 135 and 136 isobaric chains, one might expect possible perturbations in the primary product yields if nuclear shell structure were influencing the final product distribution. No noticeable deviations from a smooth Gaussian function were observed for the excitations studied. This can be taken to mean that the importance of shell structure has been reduced to a minor level. Colby and Cobble[59] have investigated the independent yields of a few isotopes with one neutron beyond a closed neutron shell. Their conclusions were that these isotopes had abnormally low yields. However, these conclusions were based upon some prescription for predicting Z_p of the particular chain, and thus, as contrasted with our results, were not independent of the assumptions involved in the prescription. If their interpretation were correct, Xe^{137} which has an appreciable independent yield ($\approx$ 30% of chain yield for some of these energies) would lose a major portion of its yield to Xe^{136}. A change of this order in the Xe^{136} cumulative yield would be easily discernable and was not observed.

2. Empirical Z_p's and Neutron Emission.

The charge-distribution function for the 135 isobaric chain is uniquely determined from data alone, and is not the result of a correlation

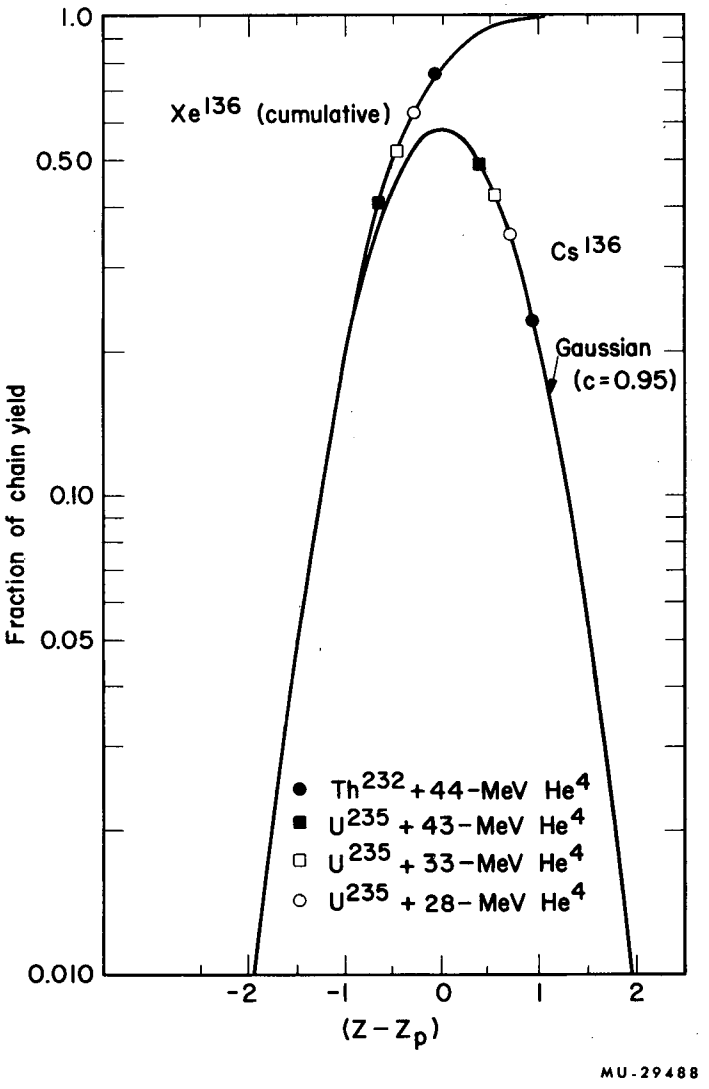

Fig. 7. Fractional yields of Xe^{136} and Cs^{136} as a function of $(Z-Z_p)$. The Xe^{136} cumulative yield is based on the mass-136 chain yield obtained from an extrapolation of lighter-mass Xe chain yields. The Cs^{136} fractional yields for $U^{235}(He^4,F)$ are those of reference 58.

of fractional yields from different masses based on a Z_p prediction. Therefore it is instructive to approach the problem of charge division in a manner similar to Wahl's[34] treatment of thermal-neutron fission of U^{235}. That is, Z_p values for chains in which the fractional yield of only a single member is known may be estimated from the charge-distribution curve previously described, by letting the single fractional yield fix the value of $(Z-Z_p)$, and thus Z_p. An assumption that is automatically injected into the discussion is that the charge dispersions in all mass chains are identical. This appears to be a good assumption in view of the results of other workers,[26] and indirectly, from the observation of the invariance of the dispersion with excitation energy.

The fractional chain yields of shielded isotopes measured in this work, and the empirical Z_p's for those chains are summarized in the Appendix. The energy dependence of Z_p for fission resulting from the excited U^{236*} compound nucleus ($Th^{232} + He^4$ and $U^{235} + n$) can now be investigated. Figure 8 is a plot of Z_p vs the excitation in U^{236*}. If an empirical Z_p is known in neutron fission of U^{235} for the masses listed, it is also incorporated in the plot. Above approximately 23-MeV excitation, it can be seen that the Z_p's of the heavy-mass chains vary with energy in similar ways. It is likely that above this energy the fission process has "established" itself. That is to say, the distribution of nuclear charge between the primary fragments is now controlled by a process which is unaltered by additional excitation in the compound nucleus; therefore, the resultant change in Z_p with energy is due only to increased neutron emission at the higher excitations. This smooth and similar variation in Z_p with energy adds support to the assumption of an identical charge dispersion in all mass chains. The fractional chain yields of the separate mass chains are varying over different regions of the charge-distribution curve, yet they still predict the same change in Z_p for a given change in energy. This means that the actual dispersion is identically equal in all isobaric sequences. At lower excitations (below $\approx$ 23 MeV) a more rapid change of Z_p with energy is observed for the mass-130 and -136 chains. These yields are in the same mass region as the supposedly nuclear-shell-

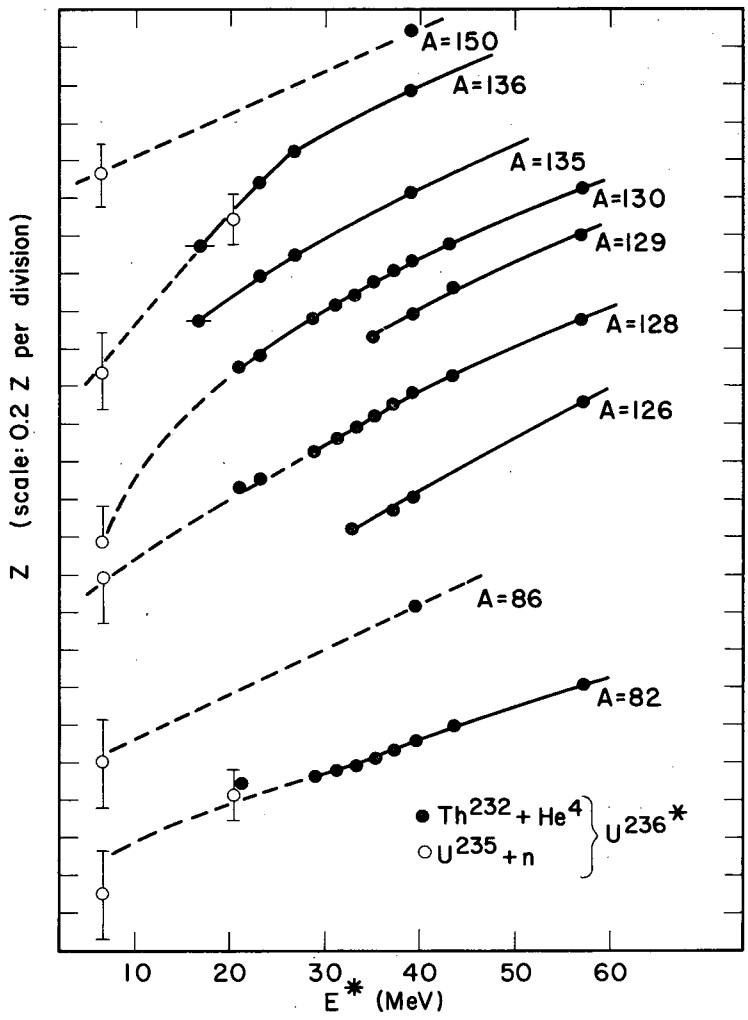

Fig. 8. Empirical Z_p's for the fission of U^{236*} as a function of excitation energy. The $U^{235}(n_{th},F)$ empirical Z_p's are taken from Wahl et al.,[26] except Pm^{150}. The Pm^{150} fractional chain yield of Chu[21] has been corrected for Pm^{150} formed by $Sm^{149}(n,\gamma)Pm^{150}$. The $U^{235}(n_{14MeV},F)$ empirical Z_p's were derived from data in reference 25.

influenced yields produced in the fission of U^{235} by thermal neutrons. It is therefore likely that the same factors which depressed the thermal-neutron U^{235} yields are causing the rapid drop of Z_p at these masses as the excitation is lowered.

If we return to the region above $E^* \approx 23$ MeV for Z_p vs E^*, we can obtain some information concerning the rate of neutron boil-off as a function of excitation energy. Since

$$\left(\frac{\partial Z_p}{\partial E}\right)_A = -\left(\frac{\partial Z_p}{\partial A}\right)_E \left(\frac{\partial A}{\partial E}\right)_{Z_p}$$

and $$\left(\frac{\partial A}{\partial E}\right)_{Z_p} = -\left(\frac{\partial \nu}{\partial E}\right)_{Z_p} ,$$

then $$\left(\frac{\partial \nu}{\partial E}\right)_{Z_p} = \frac{\left(\frac{\partial Z_p}{\partial E}\right)_A}{\left(\frac{\partial Z_p}{\partial A}\right)_E} .$$

The quantity $(\partial Z_p/\partial A)_E$ can be approximated by noting that Z_p closely parallels Z_A, the most stable charge associated with mass number A.

or $$\left(\frac{\partial Z_p}{\partial A}\right)_E \approx \left(\frac{dZ_A}{dA}\right) \approx 0.38^*,$$

$$\left(\frac{d\nu}{dE}\right) \approx \frac{\left(\frac{\partial Z_p}{\partial E}\right)_A}{0.38} .$$

The average for $(\partial Z_p/\partial E)_A$ in the mass chains closest to symmetry (see Fig. 8, A = 128 to 138) is 0.026 MeV^{-1}. Since this represents just the

---

* An average value for the mass regions stated.

change for one fragment and the complementary fragment variation is not known, we approximate the total $d\nu_T/dE$ by taking twice the single fragment change:

$$\frac{d\nu_T}{dE} \approx 2\left(\frac{d\nu}{dE}\right) \approx 0.136 \text{ MeV}^{-1}.$$

For a symmetric split, twice the single fragment change should precisely equal $d\nu_T/dE$. A value of $d\nu_T/dE = 0.12$ MeV^{-1} was obtained by Leachman[60] from an analysis of the number of neutrons measured experimentally in fission induced by 0- to 14-MeV neutrons. From a correlation of all fission data through ≈ 35-MeV excitation, Powers[61] derived a value of 0.134 MeV^{-1}. Our result can be considered in good agreement with these values. It will be shown later that there is strong evidence the light fragments emit fewer neutrons than the heavy at higher excitations, thus improving the agreement in $d\nu_T/dE$.

Figure 9 shows a plot of Z_p vs He^4 bombarding energy, constructed from results for the He^4-induced fission of U^{235}. Thorium and uranium show the same dependence of Z_p with excitation. In addition, they both show that the Z_p of the light masses (around 82) vary more slowly with E^* than do the Z_p's of the heavy masses. To illustrate this point a bit more dramatically we have plotted in Fig. 10 the fractional chain yield ratio of I^{128}/Br^{82} for a number of energies. We chose I^{128} as the heavy-mass representative because it has approximately the same fractional chain yield as the Br^{82}. If we believe (as was inferred from Fig. 8) that in fission the division of nuclear charge between the primary fragments is independent of excitation at these energies, the only factors that could contribute to the I^{128}/Br^{82} energy dependence are: (1) the charge dispersions in the two mass chains are not identical, and (2) the heavy fragment $d\nu/dE$ is greater than that of the light fragment. Factor (1) is totally inconsistent with our earlier reasoning. In addition, if the distribution were wider for mass 82, which has to be the case if the effect is in the dispersions, the empirical Z_p—predicted from the fractional chain yield

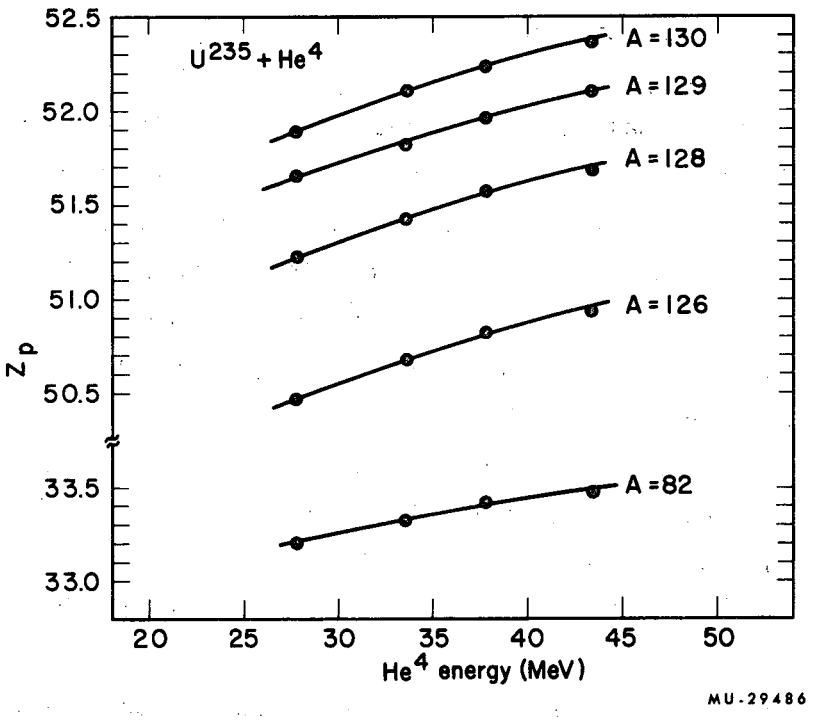

Fig. 9. Empirical Z_p's for $U^{235}(He^4,F)$ as a function of the He^4 bombarding energy.

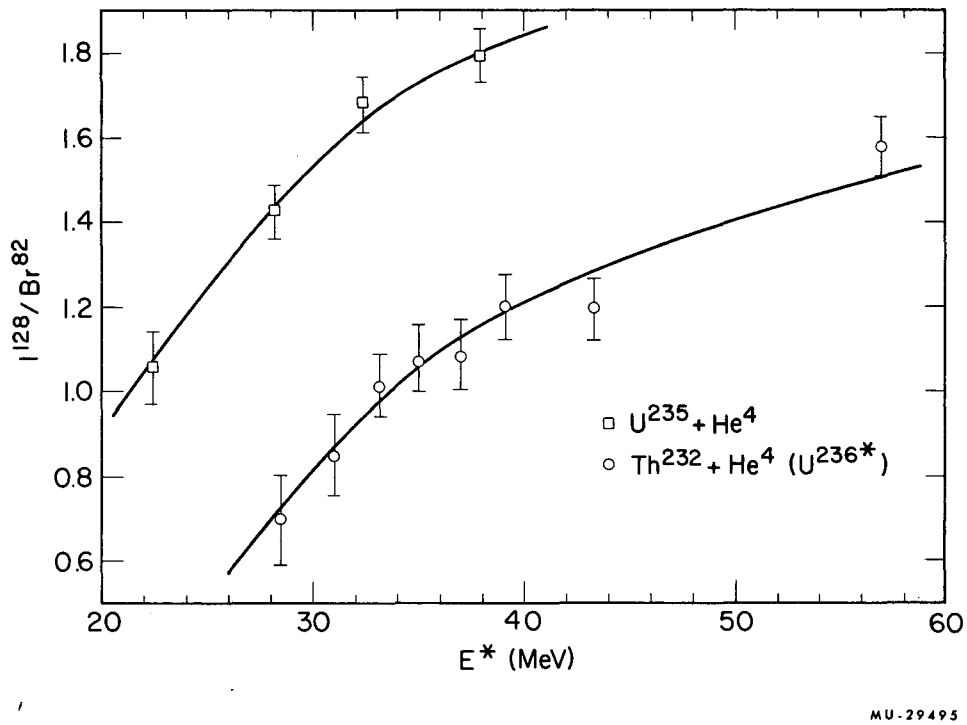

Fig. 10. Fractional chain yield of I^{128} relative to the Br^{82} fractional chain yield as a function of excitation energy for $Th^{232}(He^4,F)$ and $U^{235}(He^4,F)$.

and the wider dispersion--would be lowered. The Z_p predicted for this mass on the basis of our Gaussian of c = 0.95 is already unusually low if the $d\nu/dE$ of the heavy and light fragments are the same. We are left with factor (2) being the more plausible. The $d\nu/dE$ varies, depending on the mass region. It is conceivable that the two listed factors could both contribute to the variation; however, the dominating contributor should be $d\nu/dE$.

The empirical Z_p's for the He^4-induced fission of Th^{232} and U^{235} are plotted as $Z_p - 0.4A$ vs mass number A in Fig. 11. The mass number A is the product after neutron emission. The expanded charge scale $Z_p - 0.4A$ was suggested by Coryell[35] so that any structure in the Z_p function would be easily observed.

From Fig. 11 it is shown that a smooth non-wiggly line can be drawn consistent with the data for each case. The resulting lines define the Z_p functions for the two systems. The extrapolation in the intermediate-mass region can be justified by a number of reasons. The accuracy of our data is such that the trends shown for the Z_p's in the light- and heavy-mass regions are unquestionable. (The error bars placed on the data points in Fig. 11 represent the maximum possible error from all sources (assumptions, etc.) in each point. The data alone warrants much lower error limits.) This, together with the fact that structure in the Z_p function for the mass-128 to 136 region has disappeared (see Fig. 16) compared to low-energy fission supports the smooth joining of the curves for the two regions. The Z_p function in the intermediate region is in agreement with the energetics involved. One expects from our earlier results for $d\nu_T/dE$ and the results of other workers[60,61] that at about 40-MeV excitation a total of about seven neutrons should be boiled off per fission. The fact that these are in agreement will be shown next.

It is possible from the Z_p function alone to extract information concerning the total number of neutrons, ν_T, emitted per fission as a function of the mass split. For a pair of complementary fragments the values $h = Z_{p_H} - 0.4A_H$ and $\ell = Z_{p_L} - 0.4A_L$ can be obtained from Fig. 11.

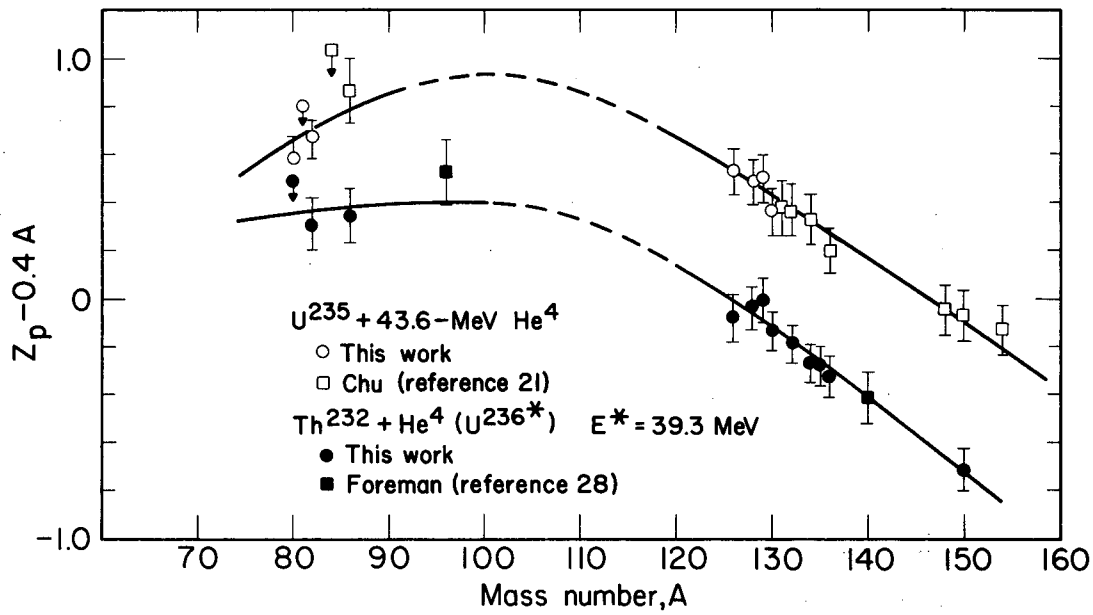

Fig. 11. Empirical Z_p's vs mass number A.

If we assume no charged particles emitted at these excitations, then $Z_{p_L} + Z_{p_H} = Z_C$ and $A_L + A_H = A_C - \nu_T$, where Z_C and A_C are the charge and mass of the compound nucleus, respectively. From these relationships it can be shown that for complementary fragments

$$\nu_T = \frac{0.4\, A_C - Z_C + (h+\ell)}{0.4} . \qquad (4)$$

The total number of neutrons, ν_T, was calculated from Eq. (4) as a function of the mass split by choosing approximately complementary mass fragments (±1 neutron) for the determination of h and ℓ from Fig. 11. The choice of fragment pairs depends on the total number of neutrons emitted; however, this only affects the derivation of ν_T in second order, and does not change the conclusions to be drawn.

In Fig. 12, ν_T calculated from our Z_p function is plotted vs A_H/A_C. It is readily apparent that there is a strong dependence of ν_T on mass asymmetry. Also shown is the variation of ν_T with mass ratio for the spontaneous fission of Cf^{252} as measured by Stein and Whetstone.[62] The portion of their curve given covers the mass ratios containing the great majority of fission events. The variation in ν_T observed for the spontaneous fission of Cf^{252} still appears to be a dominant feature of fission even at higher excitations. The energy partition in fission must be such that the symmetric modes receive a greater share of excitation than the asymmetric divisions.

From an analysis of cumulative yield measurements for nearly complementary masses in the deuteron-induced fission of natural uranium, Sugihara et al.[63] also observed that fewer neutrons are emitted in modes leading to highly asymmetric products compared with the most probable modes. One of Milton and Fraser's[64] interpretations of the large drop in the total kinetic energy release near symmetry for neutron fission of U^{235}, U^{233}, and Pu^{239} was based on large excitation energies at symmetry. They also pointed out that the two types of fission—symmetric fission with highly excited fragments of low kinetic energy, and asymmetric fission

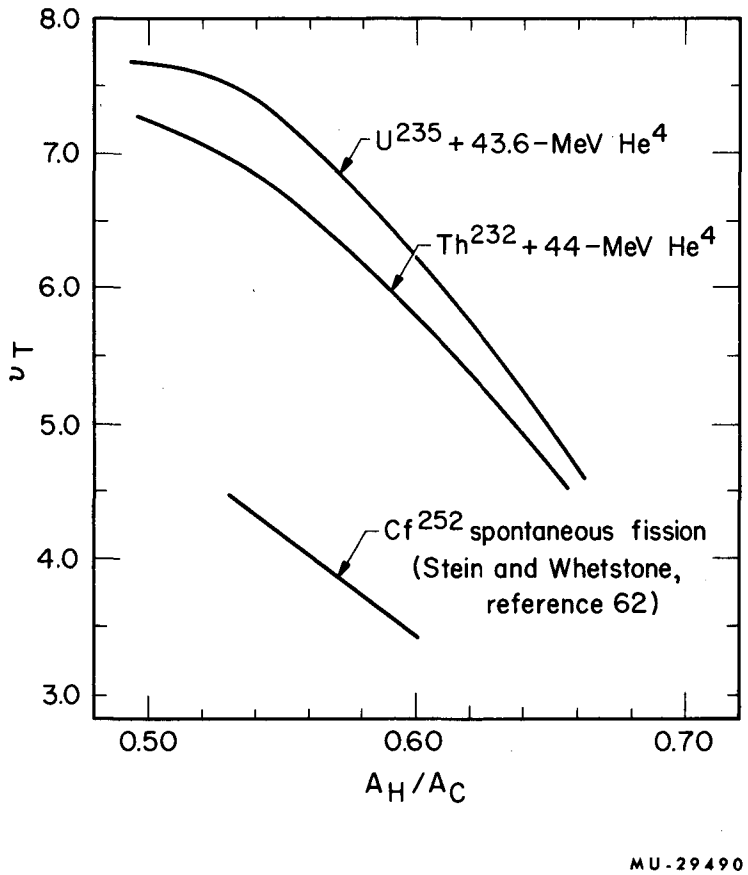

Fig. 12. Total number of neutrons emitted per fission vs the mass fraction A_H/A_C; A_H is product mass after neutron emission.

with moderately excited fragments of high kinetic energy—might be associated with the existence of two barriers and two saddle-point shapes as predicted by liquid drop calculations of Cohen and Swiatecki.[65]

It is possible to perform a total energy balance by using a suitable mass equation once the number of neutrons and the charge division for the fragment pairs are known for the system. This we hope will yield the dependence of the average total kinetic energy release on mass ratio. The energy balance can be written as

$$\langle E_k \rangle = \langle E_R \rangle - \nu_T(\langle E_B \rangle + E_{nk}) - E_\gamma ,$$

where $\langle E_k \rangle$ is the average kinetic energy of the primary fragments, $\langle E_R \rangle$ is the average total energy release, and $\langle E_B \rangle$ is the average neutron binding energy for a particular fragment pair. The quantities E_{nk} (neutron kinetic energy) and E_γ (gamma energy) were assumed to be independent of mass, and were given the values used by Milton and Fraser:[64] $E_{nk} \approx 1.2$ MeV and $E_\gamma \approx 7.5$ MeV. The dependence of ν_T on mass ratio was that of Fig. 12.

Figure 13 shows the average total kinetic energy release, $\langle E_k \rangle$, as a function of the heavy-fragment mass calculated for fission on Th^{232} induced by 44-MeV He^4. Curve A is based on Cameron's mass formula.[67] The tables of Milton[68] were used to determine $\langle E_R \rangle$ and $\langle E_B \rangle$ for the charge division predicted by our Z_p function. In these tables $\langle E_R \rangle$ and $\langle E_B \rangle$ have been averaged over a Gaussian charge distribution similar to that measured in this work. Curve B is based on the energy release given by Green's[69] liquid drop mass formula and our Z_p function. For this case an average neutron binding energy for all masses was assumed as $\langle E_B \rangle \approx 5.6$ MeV in order to be consistent with the liquid drop interpretation.

No strong conclusions can be drawn from the results in Fig. 13. However, one can notice that the shell-affected mass formula yields a dependence of $\langle E_k \rangle$ similar to low-energy fission; whereas, the liquid drop model shows a variation resembling higher-energy results.[70]

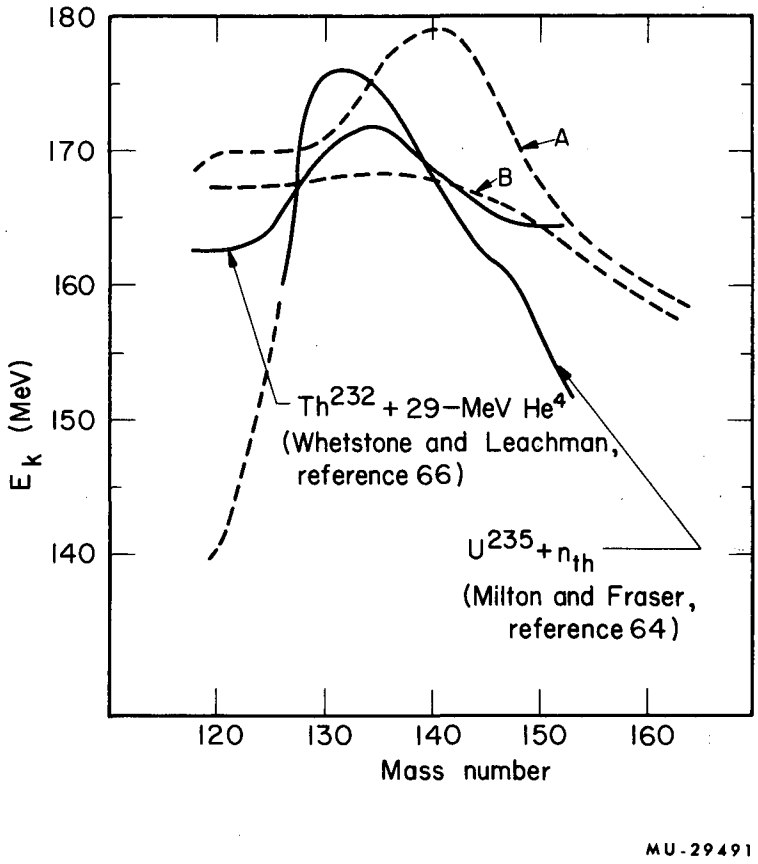

Fig. 13. The average total kinetic energy as a function of the heavy-fragment mass. Curve (A) is calculated from Cameron's[67] masses and curve (B) from Green's[69] masses for Th^{232} (44-MeV He^4,F).

3. Minimum Potential Energy (MPE) Treatment of Charge Division.

Once the Z_p function has been determined, the next logical step is to seek an explanation or mechanism for the observed division of charge between fragment pairs. The unchanged charge distribution (UCD) hypothesis which enjoyed success for 190-MeV deuteron fission of Bi^{209} (Goeckermann and Perlman[71]) has not received any substantial support for intermediate-energy fission.[21,58,72-74] According to this hypothesis, the primary fission fragments have the same neutron-to-proton ratio as in the fissioning nucleus. The UCD hypothesis predicts values of Z_p for the extremely asymmetric mass splits (this is the most sensitive region) that are inconsistent with our results. The charge-to-mass ratios predicted for the heavy fragments are much greater than observed.

Two other postulates which prescribe the manner in which nuclear charge is to be divided in fission are the equal charge displacement (ECD) hypothesis, and the minimum potential energy (MPE) theory. The ECD hypothesis was an empirical suggestion by Glendenin et al.[30] which stated that the most probable charges for one fission fragment and for its complementary fragment lie an equal number of charge units away from beta stability. The MPE theory proposes that a nucleonic redistribution occurs such that a minimum in the sum of nuclear potential energy and Coulombic repulsion energy is attained. Because the ECD and MPE treatments yield almost similar results for a particular mass formula,[36] we chose the MPE for its theoretical basis—and also for the reason that our results suggested a mechanism that gives the light fragment more than its share of charge, and the heavy fragment less.

The basic ideas embodied in the MPE theory were first proposed by Present.[75] The later MPE formulations of Swiatecki[76] were employed by Blann[36] to describe successfully the charge division for the fission of Au^{197} with 112-MeV C^{12} ions. We will use the MPE treatment, as did Blann, in the framework of the liquid drop model. That is, a liquid drop mass formula (Green[69]) is used to describe the nuclear potential energy surface.

The total energy for a fragment pair can be written

$$\text{P.E.} = M_L + M_H + \frac{Z_H Z_L Q^2}{D}, \qquad (5)$$

assuming the configuration at scission can be represented by tangent spheres, where D is the effective separation of the fragment centers; M_L, M_H, Z_L, and Z_H are the mass and charges for the heavy and light fragments; and Q is the unit of elemental charge. Green's mass formula is[69]

$$M\text{-}A = \alpha A + \beta Z + a_2 A^{2/3} + a_3 Z^2 A^{-1/3} + a_4 (A-2Z)^2 (4A)^{-1}. \qquad (6)$$

The constants given by Green are: $a_2 = 17.97$, $a_3 = 0.718$, and $a_4 = 94.07$ MeV. Substituting the mass formula into Eq. (5) and minimizing $(\partial \text{P.E.}/\partial Z_L = 0)$ with the constraint $Z_L + Z_H = Z_C$, the compound nucleus charge, one obtains for Z_{p_L} (before neutron boil-off from fragments)

$$Z_{p_L} = \frac{Z_C \left(a_4 A_H^{-1} + a_3 A_H^{-1/3} - \frac{1}{2} Q^2 D^{-1}\right)}{a_3 \left(A_L^{-1/3} + A_H^{-1/3}\right) + a_4 \left(A_H^{-1} + A_L^{-1}\right) - Q^2 D}. \qquad (7)$$

Milton[68] developed a similar expression for Z_{p_L}, except that his expression contained additional parameters to account for any spheriodal deformation of the fragments at scission. In this work the effective separation of the fragment centers D was chosen so that the $Z_H Z_L Q^2/D$ term of Eq. (5) would yield the correct total kinetic energy release. The kinetic energy release is dependent on the mass ratio of the fragments; therefore, an average value for D was taken (D =18F) and held constant in Eq. (7).

In order to interpret gainfully the predictions of Eq. (7) as regards the experimentally determined Z_p's, one must know how many neutrons were emitted from the individual primary fragments. Our earlier discussions showed that the total number of neutrons, ν_T, emitted per fission

was dependent on mass asymmetry. This observation, along with some assumption concerning the partition of ν_T between the light and heavy fragments, could be used (as is the usual case in a study of charge distribution) to test the validity of a proposed charge-division prescription by comparing with the experimentally derived Z_p's. However, the assumptions relating to the partition of ν_T at these higher excitations possesses no more strength than the Z_p prescription itself. It is therefore proposed that we assume the MPE treatment predicts the exact charge division for the primary fragments, and that from the empirical Z_p's we determine the neutron yields ν_A for the individual fission fragments.

In Figs. 14 and 15 the MPE Z_p functions for 4, 3, 2, and 1 neutron being boiled out of the primary fragments are shown along with the empirical Z_p's for the two cases. Also shown are the predicted ν_A's. For Th^{232} + 44-MeV He^4 and U^{235} + 43.6-MeV He^4 the average fissioning nuclei were taken as U^{235} and $Pu^{238.5}$, respectively. These were chosen so as to be consistent with the branching ratios for neutron emission and fission, Γ_n/Γ_f, given by Vandenbosch et al.[77] and Foreman[28] for these compound systems.

Our results indicate that the sawtooth variation of neutron yields[78,79] with fragment mass observed for spontaneous and thermal-neutron fission disappears in higher-excitation fission. Although the corresponding light-mass regions show a similar variation, the effect in the lightest heavy fragments has been completely "washed out." For low-energy fission, the minimum in the fragment neutron yield is found in the neighborhood of $N \approx 50$ and $Z \approx 50$ (masses 82 and 128). Terrell[80] suggested that these magic or near-magic fragments have low excitations and consequently emit almost no neutrons, because of greater rigidity against distortion from near-spherical shapes. This interpretation could be applied to higher-excitation fission in the light-mass region ($N \approx 50$); however, the products near $Z \approx 50$ are no longer formed with low excitations. The fact that an appreciable portion of higher-excitation-fission events come from symmetric modes may influence the neutron yields (excitation) more near $Z \approx 50$ than near the $N \approx 50$ region.

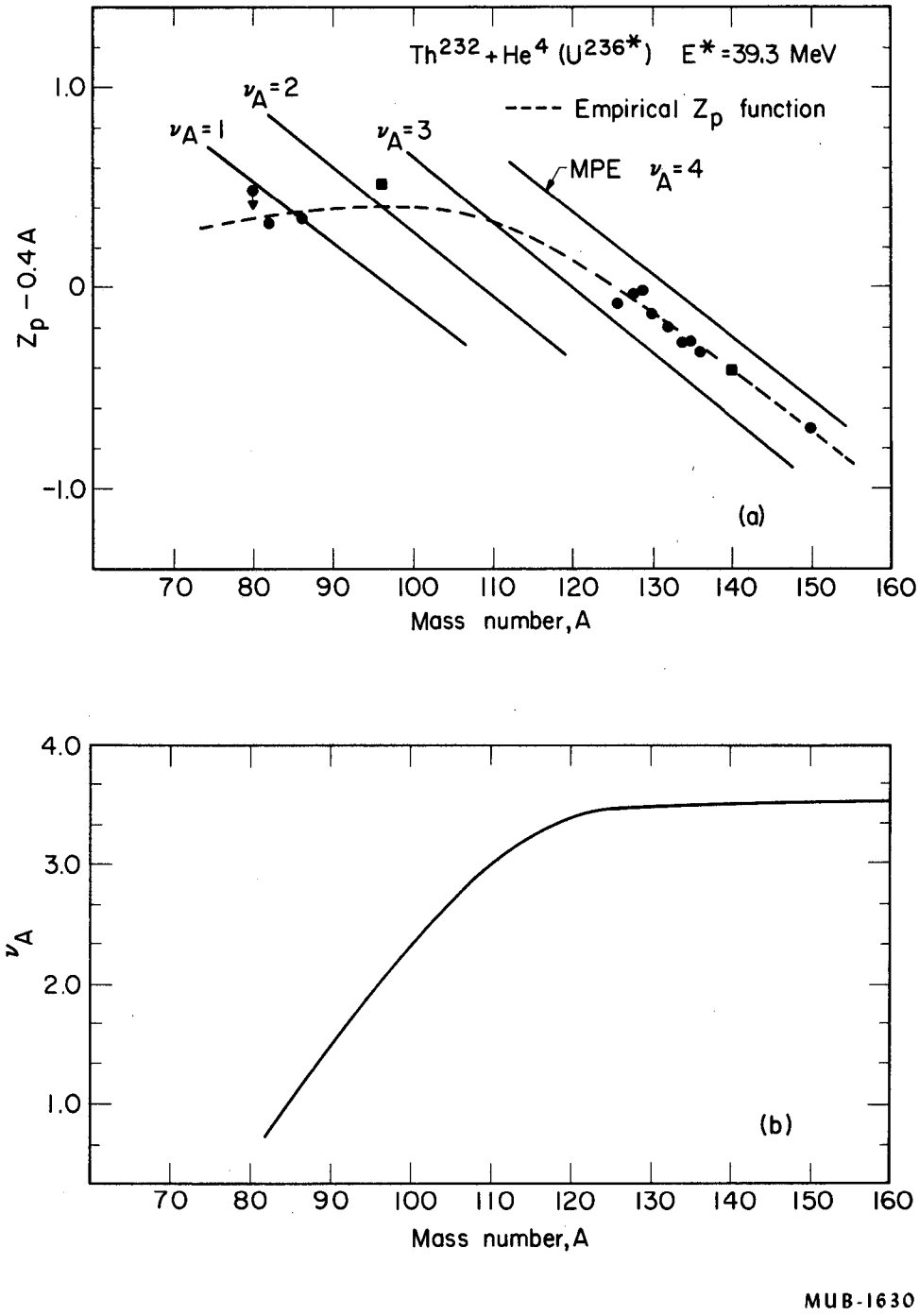

Fig. 14. (a) The most probable charge, Z_p, in fission of Th^{232} induced by He^4, based on MPE for the emission of 4, 3, 2, and 1 neutron from the primary fragment. (Points are indicated as in Fig. 11.)

(b) The fragment neutron yields ν_A needed to fit the empirical Z_p function by MPE. The average fissioning nucleus was taken as U^{235}.

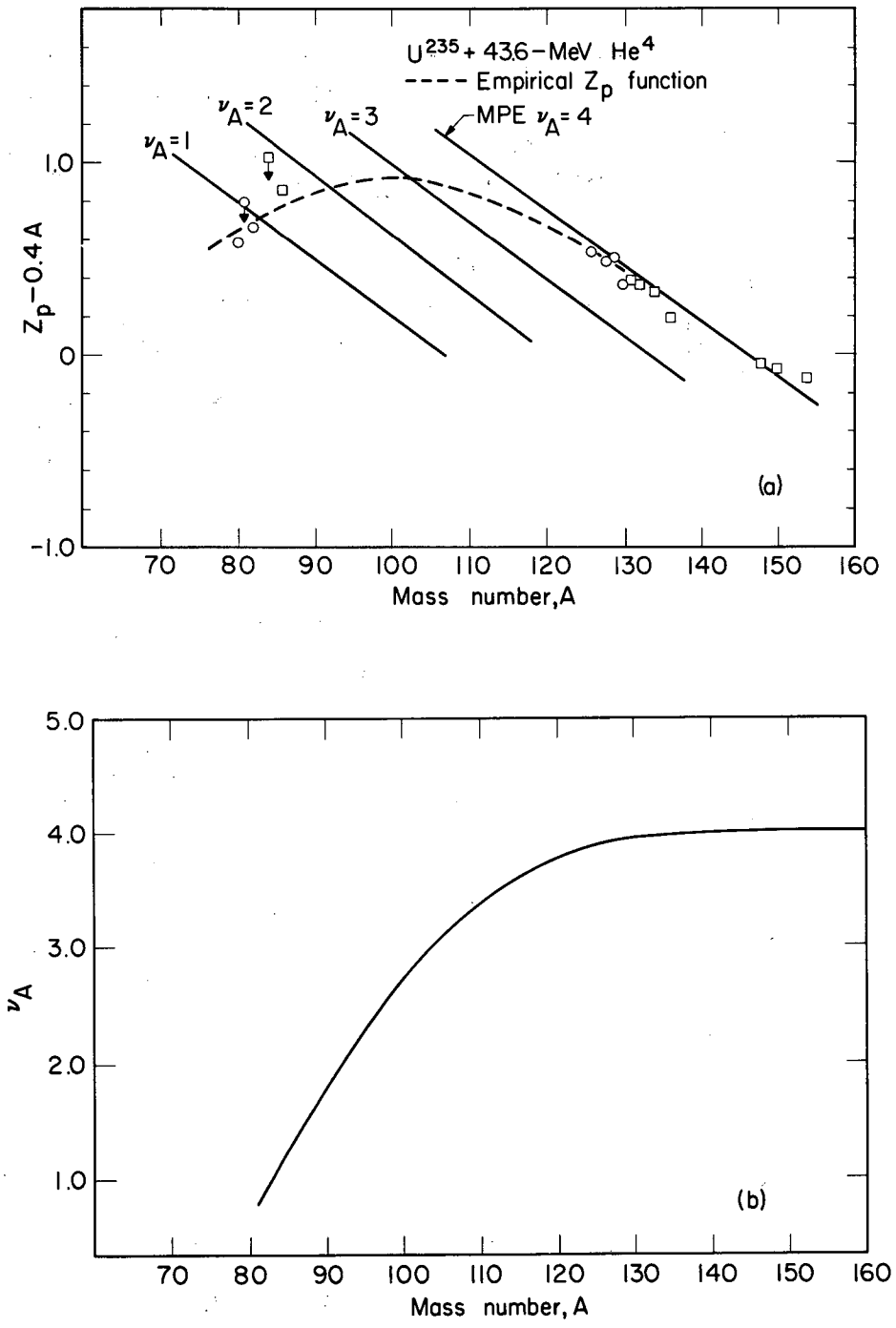

Fig. 15. (a) The most probable charge, Z_p, in fission of U^{235} induced by He^4, based on MPE for the emission of 4, 3, 2, and 1 neutron from the primary fragment. (Points are indicated as in Fig. 11.)

(b) The fragment neutron yields ν_A needed to fit the empirical Z_p functions by MPE. The average fissioning nucleus was taken as $Pu^{238.5}$.

Since the primary product neutron yields are known for the thermal-neutron fission of U^{235}, and, in addition, there is a large body of empirical Z_p's for the system, one can meaningfully test the validity of various charge-division prescriptions. Figure 16 shows the empirically determined Z_p's and Z_p functions for U^{235} (n_{th},F) and Th^{232} (44-MeV He^4, F), along with the predictions of UCD (curve A) and MPE (curve B) for U^{235} (n_{th}, F). The number of neutrons emitted by a fragment was taken from a straight line fitted to Terrell's[80] corrected experimental data for U^{235}(n_{th}, F). In the region near symmetry, the light- and heavy-fragment neutron yields were joined by a smooth curve. The MPE curve is derived by using Green's[69] mass formula and an effective fragment separation (D) of 18 F. The MPE Z_p function fits the average trend of the empirical Z_p's very well. The UCD does not at all predict reasonable Z_p's (as has been observed before).

Coryell et al.[35] have proposed a method for deriving the Z_p of any isobaric chain for various types of fission differing in compound nucleus and in excitation energy. Their expression uses the Z_p function for U^{235}(n_{th}, F) as a basis function for all computed Z_p's. The shift in the Z_p function, $\Delta Z_p(A)$, by their method is dependent only on Z_C, A_C and ν_T, the charge and mass of the compound nucleus, and the total number of neutrons boiled out per fission. This method is inapplicable at higher excitations for two reasons: (a) no structure similar to U^{235}(n_{th}, F) remains in the Z_p function at higher excitations, and (b) the shift in Z_p due to increased excitation is not the same for all mass chains, as is implied by their prescription.

The foregoing results and discussion of charge distribution strongly suggest the need for a direct experimental determination of fragment neutron yields for fission induced by charged particles. A measurement of this type will remove the major obstacle in the path of answering the question of how nuclear charge is divided in fission at these excitations. We feel that our indirectly determined neutron yields will be verified, and thus will establish the validity of the MPE treatment of nuclear charge division in fission.

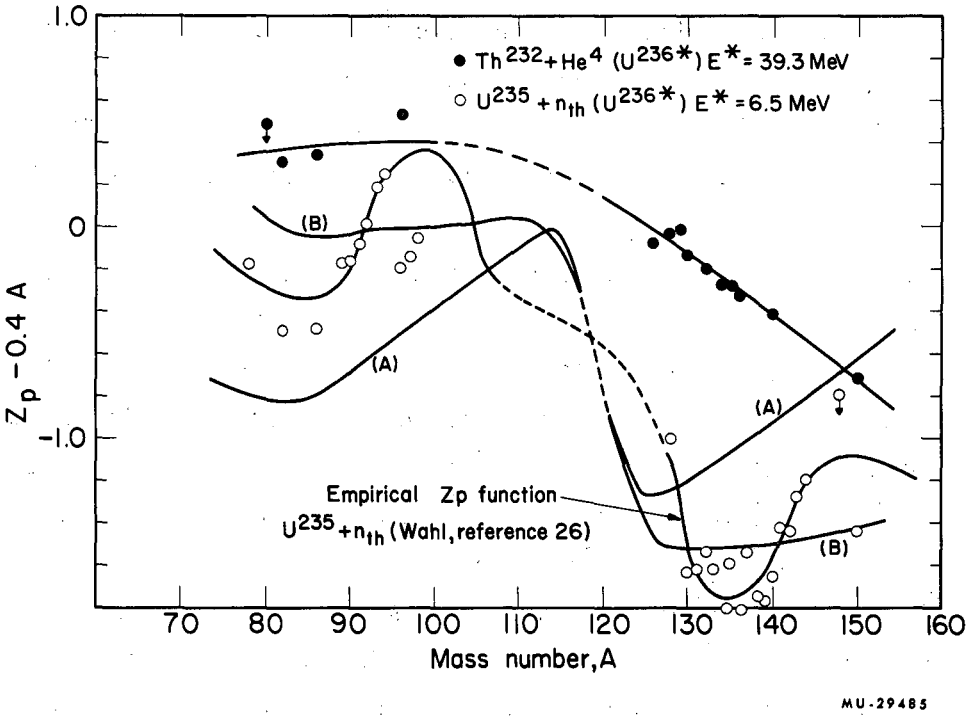

Fig. 16. The empirical Z_p's for U^{236*} are compared; and the comparison of empirical Z_p's for $U^{235}(n_{th},F)$ with those predicted by UCD curve (A) and MPE curve (B) are made.

4. Population of Kr^{85} Isomeric States in Fission.

We observed that as the excitation energy in the compound nucleus increased, the amount of fission-produced $Kr^{85}(t_{\frac{1}{2}} = 10\ yr,\ I = 9/2)$ increased relative to the total mass-85 chain yield. For thermal-neutron fission of U^{235} in which the independent yield of Kr^{85} is negligible, all the mass-85 yield decays through $Kr^{85m}(t_{\frac{1}{2}} = 4\ h,\ I = \frac{1}{2})$. The 4-h state branches such that 21.9% of the decays go to the 10-yr ground state,[81] and the remainder decays to Rb^{85}. So if the total 85 chain yield (including the independent yield of Kr^{85}) populates Kr^{85m}, the observed Kr^{85} (10-yr) relative to the mass-85 chain yield would equal 0.219. Figure 17 shows the observed Kr^{85} (10 yr) relative to the mass-85 chain yield as a function of energy for the helium-ion-induced fission of Th^{232} and U^{235}. The energy dependence for the observed ratios is related to the amount of independently formed Kr^{85}. An expression for the branching from Kr^{85m}(BR) can be derived from our results (OBS), the fractional chain yield of Kr^{85}(FCY), and the fraction of Kr^{85} that populates the ground state (a):

$$\frac{OBS - a(FCY)}{1 - a(FCY)} = BR. \qquad (8)$$

Now we can determine a, since the branching is known from other sources[81] (BR = 0.219) and the FCY can be predicted from the Z_p function, dZ_p/dE, and the Gaussian charge dispersion. Upon performing this operation, it is found that $a \approx 1$. In order to illustrate this, we choose a = 1 and calculate a BR according to Eq. (8). The calculated BR's are designated "corrected points" and are shown in Fig. 17; they are tabulated in Table XI for $U^{235}(He^4,F)$. The error bars on the corrected points represent the uncertainty in FCY. It is readily apparent from the agreement between the corrected points and the expected branching that the majority ($a > 90\%$) of the independently formed Kr^{85} populates the high-spin isomer.

Biller[82] measured several isomer cross sections from 340-MeV proton fission of bismuth, and found that in all cases the high-spin isomer was formed in greater yield. Hicks and Gilbert,[83] and a number of other

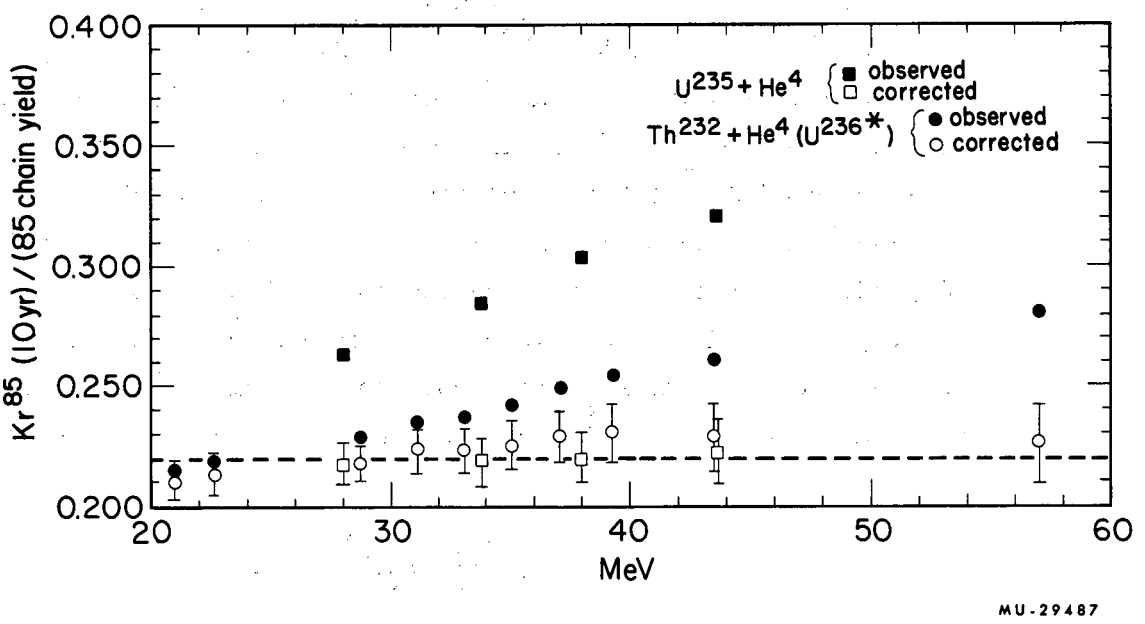

Fig. 17. The dependence of the 10-yr Kr^{85} isomer yield relative to the mass-85 chain yield on the excitation energy for U^{236*} and the He^4 bombarding energy for $U^{235}(He^4,F)$. The dashed horizontal line represents the expected ratio if all of mass-85 yield populates Kr^{85m}.

Table XI. Fraction of mass-85 chain produced as Kr^{85}(10 yr) for He^4-induced fission of U^{235}.

He^4 energy (MeV)	Fraction produced as Kr^{85}(10 yr)[a]	Fractional chain yield of Kr^{85}	Calculated branching[b]
43.6	0.320	0.127	0.222±0.012
38.0	0.303	0.108	0.219±0.010
33.8	0.284	0.085	0.218±0.009
28.0	0.263	0.059	0.217±0.006

[a] Obtained from data of Table VI.

[b] Based on a = 1, Eq. (8).

workers (see reference 84 for a review), supported Biller's observations. However, it is difficult to say from these results (and our results) whether the population of high-spin states is an intrinsic property of fission, or characteristic of the deexcitation from a highly excited species independent of its production. Whichever the case, it cannot be denied that the deexcitation of the primary fragment (neutron or γ) must occur from high angular-momentum states.

B. Mass Distribution

1. Yield-Mass Curve.

The yield-mass distribution is still predominantly asymmetric at 39-MeV excitation. A yield-mass curve for U^{236*} ($E^* = 39.3$ MeV) is shown in Fig. 18. The curve in the symmetric region was derived from an extrapolation of the higher-mass yield results, and a radiochemically measured valley-to-peak ratio.[29] The ordinate was adjusted so that the total area under the curve integrated to $\approx 200\%$; thus it now represents the approximate fission yield (%). Since there are not enough data in the light-mass region, we cannot determine the number of neutrons emitted as a function of mass ratio by reflection of the fission yields. Davis[29] observed upon folding his radiochemical cumulative yield results for Th^{232}(39-MeV He^4,F) that about five neutrons were emitted per fission. He also noted that this was low compared to what is expected at this excitation. However, these results were based on mass reflections for quite asymmetric fission modes and, therefore, would only yield ν_T for this region. As demonstated in this work, ν_T is dependent on mass ratio, and decreases as the asymmetry of the mode is increased. The value of about five neutrons obtained by Davis[29] is in good agreement with the values derived for these mass ratios in our earlier discussions.

The "fine structure" observed for the Xe cumulative yields[12] in the thermal-neutron fission of U^{235} is nonexistent in charged-particle-induced fission (see Fig. 19). One prominent feature of the yield-mass

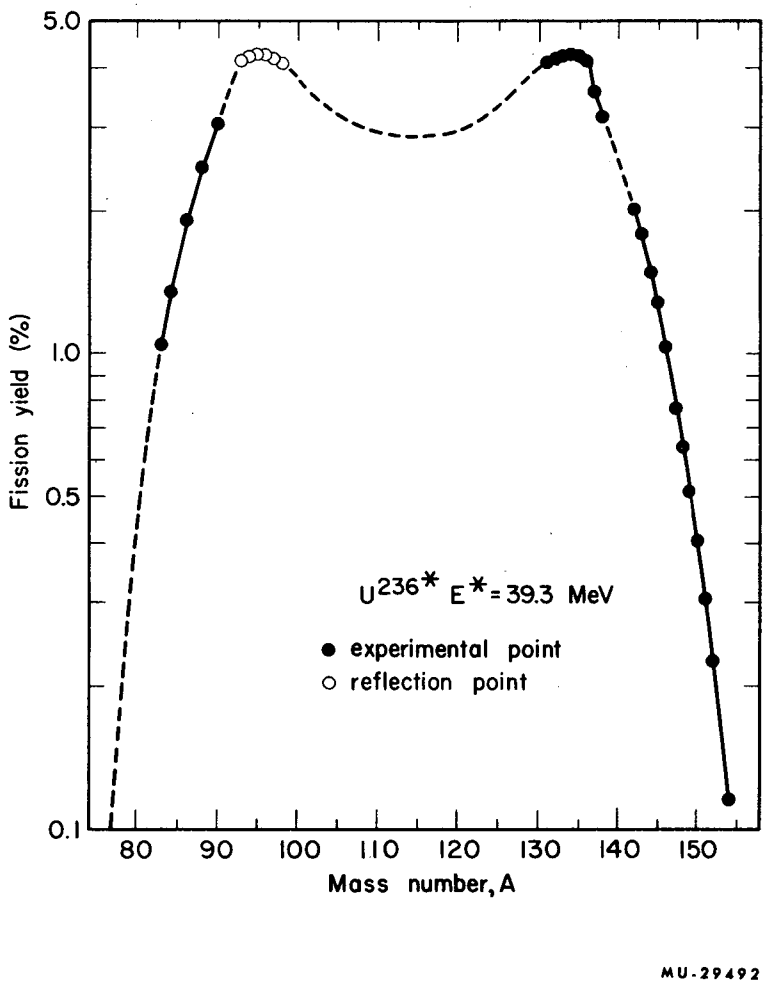

Fig. 18. Yield-mass curve for fission of Th^{232} with 44-MeV He^{4}.

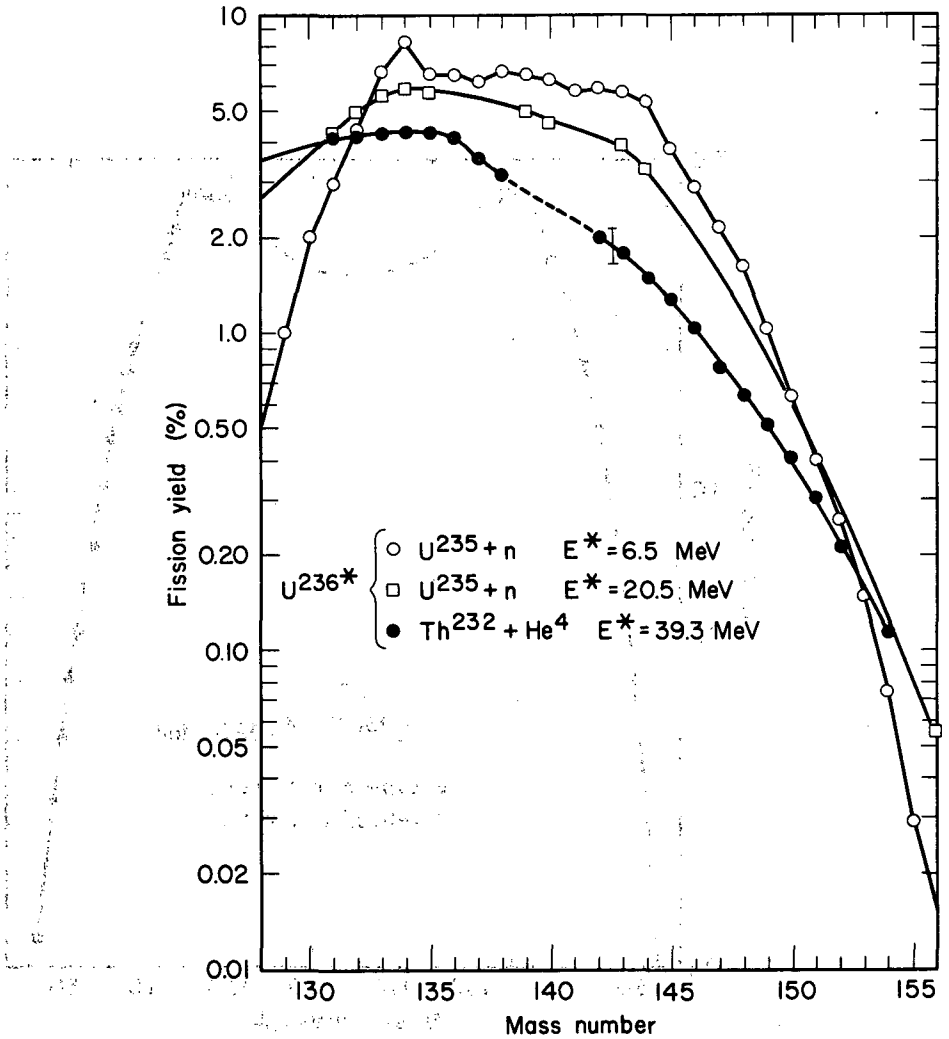

Fig. 19. Heavy wing of the yield-mass curve for U^{235}+ thermal neutrons (reference 24), U^{235}+ 14-MeV neutrons (reference 25), and Th^{232}+ 44-MeV He^4. The error bar shown indicates the uncertainty in the normalization of the rare-earth relative yields to the Xe relative yields.

curve is the rapid drop in the mass-137 and 138 yields. The rate at which these yields are decreasing is greater than the rate for the light rare earths. A possible structural preference in the fission act, or a variation in neutron emission from the primary fragments could account for this.

2. Independent Yield Distribution for Isotopes of a Given Z.

The relative independent yields of Cs, Xe, and I isotopes provide enough information for deriving a distribution function for the independent yields of isotopes of a given Z. In Table XII the relative independent yields are listed for the highest-energy helium-ion-induced fission of U^{235} and Th^{232}. All yields are relative to the mass-131 total chain yield. Since the yield-mass curves are nearly level in this region, the most probable mass number, A_p, for a given charge should peak at the same value of cross section for each isotope (Cs, Xe, and I). These conditions—together with the distribution function that best fit all the results—were used to determine the A_p's for each Z.

Figure 20 shows the relative yields (y_r) of Table XII plotted vs ($A-A_p$). A Gaussian function

$$y_r \propto \exp\left[\frac{-(A-A_p)^2}{7}\right] \qquad (9)$$

gives the best fit to the data.

It can be shown that this dependence is expected in light of a Gaussian charge dispersion, and equal chain yields. The yield for independent formation of a product nuclide is given by

$$y(A,Z) = Y_A(0.95\pi)^{-\frac{1}{2}} \exp\left[\frac{-(Z-Z_p)^2}{0.95}\right], \qquad (10)$$

where Y_A is the chain yield for mass number A, and the other variables

have the usual meanings. Since it is known that the chain yields in this mass region are the same ($Y_A = Y_{A'}$), and $dZ_p/dA = 0.365$ (obtained from data in the mass region 126 to 136) or $\Delta Z_p = 0.365\ (A-A')$, the yield in some other isobaric sequence A' within this mass region is given by

$$\bar{y}(A',Z) = Y_A(0.95\pi)^{-\frac{1}{2}} \exp\left[-\frac{(Z-Z_{p_A}-0.365A+0.365A')^2}{0.95}\right]. \quad (11)$$

Upon setting $\partial y(A',Z)/\partial A' = 0$, one obtains A as a function of Z, Z_{p_A}, and A_p, where A_p is the mass (not necessarily integral) at which the yields of isotopes of a given Z have a maximum. By substituting for A in Eq.(11), the yield at constant Z becomes

$$\bar{y}_Z(A') = Y_A(0.95\pi)^{-\frac{1}{2}} \exp\left[-\frac{[0.365\ (A'-A_p)]^2}{0.95}\right], \quad (12)$$

or in general

$$\bar{y}_Z(A) \propto \exp\left[-\frac{(A-A_p)^2}{7.1}\right]. \quad (13)$$

The agreement between Eq. (9) and Eq. (13) substantiates the fact that the charge dispersion is a Gaussian of width constant 0.95.

Blann[55] observed that the distribution of independent yields of isotopes for a given Z in the 112-MeV C^{12} fission of Au^{197} could also be described by a Gaussian. However, the distribution width constant (c= 6.0) was not the same as that of the above distribution (c= 7.0). Levy and Nethaway,[85] upon an analysis of Blann's results, proposed that symmetric fission may follow a bivariate normal distribution of charge and mass. The Gaussian distribution of mass shown in our work is a consequence of the Gaussian charge dispersion, and the nature of the total mass yields.

Table XII. Relative independent yields of Cs, Xe, and I isotopes for the He^4-induced fission of U^{235} and Th^{232}.

Mass No.	Relative independent yields[a]		
	Cs[b]	Xe	I
	U^{235} 43.6-MeV He^4		
126			0.0057
128			0.0865
129		0.0121	
130			0.357[d]
131	0.0038		
132	0.0190		
134	0.191		
136	0.500	0.355[c]	
$A_p \rightarrow$	136.8	134.2	131.7
	U^{236*} 57.0-MeV excitation		
126			0.0039
128			0.0681
129		0.0085	
130			0.327[d]
136		0.390[c]	
$A_p \rightarrow$		134.4	131.9

[a] All yields relative to Xe^{131} chain yield.

[b] Relative Cs independent yields are those of N. Souka,[58] based on 0.0038 as the fractional chain yield of Cs^{131}.

[c] Corrected for small yield of precursor.

[d] Corrected for yield of daughter since I^{130} was measured in Xe.

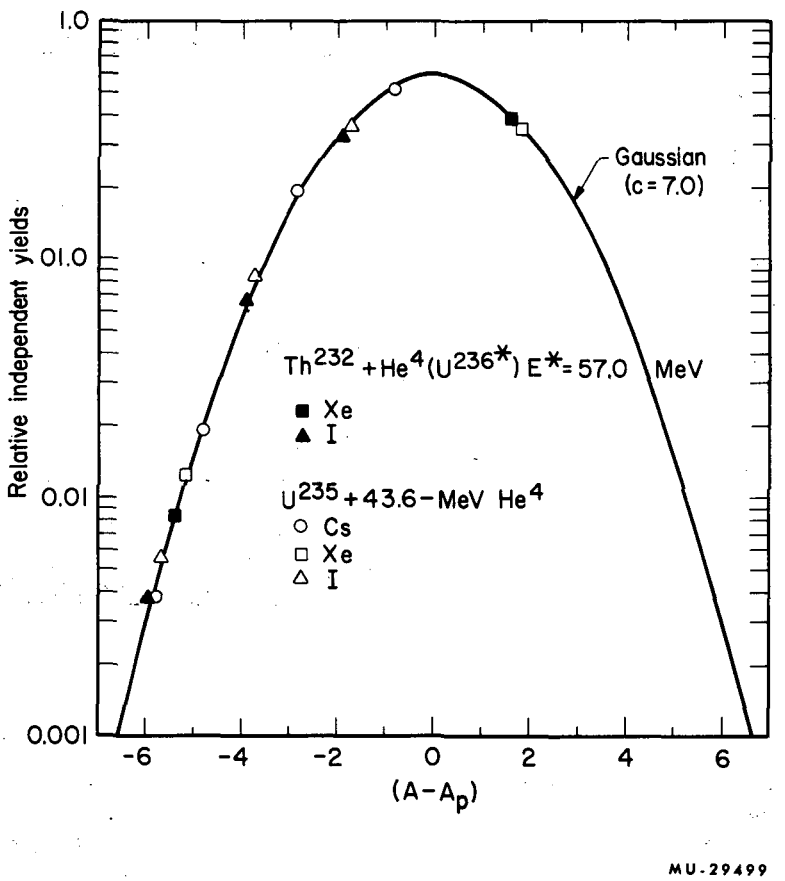

Fig. 20. Relative independent yields of I, Xe, and Cs isotopes vs mass number, $(A-A_p)$.

ACKNOWLEDGMENTS

I wish to express my appreciation to Dr. Maynard C. Michel for his guidance and assistance throughout the course of this work. I am also grateful to Professor David H. Templeton for his interest in the work reported herein.

The advice and technical assistance of Mr. Frederick L. Reynolds is greatly appreciated.

I wish to thank Dr. W. J. Swiatecki and Dr. J. M. Alexander for helpful discussions. I am grateful to Dr. W. J. Swiatecki and Dr. H. M. Blann for allowing me to quote their unpublished results, and to Mr. H. P. Robinson for assistance in the decay calculations. Discussions with Professor John H. Reynolds relating to rare-gas extraction and purification are appreciated.

Thanks are due to Messrs. George Kilian, Frederick Vogelsberg, and Milton Firth of the Electronic Support Group and Mr. Bert Watkins of Mechanical Shops for their aid in various aspects of this work.

The cooperation of Mr. Pete McWalters, Mr. John Wood, and the crew of the Crocker Laboratory 60-inch cyclotron is acknowledged.

I would like to thank Dr. Yung Yee Chu, Dr. Eldon Haines, Miss Nadia Souka, Mr. Donald Burnett, and Mr. Franz Plasil for helpful discussions.

The assistance of the Health Chemistry Group has been appreciated.

And last, but not least, I wish to thank my wife, Colette, for her encouragement and patience throughout the course of this work.

This work was performed under the auspices of the U. S. Atomic Energy Commission.

APPENDIX

Table XIII. Fractional chain yields and empirical Z_p values.

$Th^{232} + He^4$ (U^{236*})					
Excitation energy (MeV)	Isotope	Fractional chain yield	$(Z-Z_p)^a$	Z_p	$(Z_p-0.4A)$
57.0	Br^{80}	(<0.0025)	2.27	(32.73)	(0.73)
	Br^{82}	0.0400	1.59	33.41	0.61
	I^{126}	0.0039	2.18	50.82	0.42
	I^{128}	0.0633	1.45	51.55	0.35
	Xe^{129}	0.0082	2.01	51.99	0.39
	I^{130}	0.315	0.76	52.24	0.24
43.5	Br^{82}	0.0183	1.81	33.19	0.39
	I^{128}	0.0219	1.76	51.24	0.04
	Xe^{129}	0.0029	2.24	51.76	0.16
	I^{130}	0.180	1.05	51.95	-0.05

Table XII. (cont.)

Excitation energy (MeV)	Isotope	Fractional chain yield	$(Z-Z_p)^a$	Z_p	$(Z_p-0.4A)$
39.3	Br^{80}	($\leq$0.00076)	2.51	(32.49)	(0.49)
	Kr^{81}	(<0.00030)	2.68	(33.32)	(0.92)
	Br^{82}	0.0137	1.89	33.11	0.31
	Rb^{86}	0.00267	2.26	34.74	0.34
	I^{126}	0.00028	2.69	50.31	-0.09
	I^{128}	0.0165	1.84	51.16	-0.04
	Xe^{129}	0.00122	2.42	51.58	-0.02
	I^{130}	0.149	1.14	51.86	-0.14
	Cs^{132}	0.00137	2.40	52.60	-0.20
	Cs^{134}	0.0302	1.68	53.32	-0.28
	Cs^{136}	0.230	0.93	54.07	-0.33
	Pm^{150}	0.025	1.72	59.28	-0.72
37.1	Br^{82}	0.0120	1.92	33.08	0.28
	I^{126}	0.00019	2.76	50.24	-0.16
	I^{128}	0.0129	1.90	51.10	-0.10
	I^{130}	0.129	1.19	51.81	-0.19

Table XIII. (cont.)

Excitation Energy (MeV)	Isotope	Fractional chain yield	$(Z-Z_p)^a$	Z_p	$(Z_p-0.4A)$
35.1	Br^{80}	($\leq$0.00063)	2.54	(32.46)	(0.46)
	Br^{82}	0.0096	1.97	33.03	0.23
	I^{128}	0.0103	1.96	51.04	-0.16
	Xe^{129}	0.00066	2.54	51.46	-0.14
	I^{130}	0.114	1.24	51.76	-0.24
33.1	Br^{82}	0.0081	2.01	32.99	0.19
	I^{126}	($\leq$0.00011)	2.85	(50.15)	(-0.25)
	I^{128}	0.0082	2.01	50.99	-0.21
	Xe^{129}	($\leq$0.00064)	2.54	(51.46)	(-0.14)
	I^{130}	0.0957	1.33	51.67	-0.33
31.1	Br^{82}	0.0073	2.04	32.96	0.16
	I^{128}	0.0062	2.08	50.92	-0.28
	I^{130}	0.0806	1.37	51.63	-0.37
28.7	Br^{80}	(<0.00054)	2.57	(32.43)	(0.43)
	Br^{82}	0.00647	2.07	32.93	0.13
	I^{126}	($\leq$0.000054)	2.97	(50.03)	(-0.37)
	I^{128}	0.0045	2.14	50.86	-0.34
	I^{130}	0.0660	1.44	51.56	-0.44

Table XIII. (cont)

Excitation energy (MeV.)	Isotope	Fractional chain yield	$(Z-Z_p)^a$	Z_p	$(Z_p-0.4A)$
26.8	Cs^{134}	0.0076	2.03	52.97	-0.63
	Cs^{136}	0.111	1.25	53.75	-0.65
23.1	I^{128}	0.0023	2.29	50.71	-0.49
	I^{130}	0.0354	1.63	51.37	-0.63
	Cs^{134}	($\leq$0.0068)	2.05	52.59	-0.65
	Cs^{136}	0.0713	1.41	53.59	-0.81
21.0	Br^{82}	0.0056	2.10	32.90	0.10
	I^{128}	0.0019	2.33	50.67	-0.53
	I^{130}	0.0273	1.70	51.30	-0.70
15.0 to 18.0	Cs^{136}	0.0223	1.76	53.24	-1.16

Table XIII. (cont.)

He^4 Energy (MeV)	Isotope	Fractional chain yield	$(Z-Z_p)^a$	Z_p	$(Z_p-0.4A)$
		U^{235} He^4			
43.6	Br^{80}	0.0012	2.42	32.58	0.48
	Kr^{81}	(<0.00015)	2.80	(33.20)	(0.80)
	Br^{82}	0.0525	1.53	33.47	0.67
	I^{126}	0.0067	2.07	50.93	0.53
	I^{128}	0.0938	1.32	51.68	0.48
	Xe^{129}	0.0132	1.90	52.10	0.50
	I^{130}	0.376	0.64	52.36	0.36
38.0	Br^{80}	(≤0.00074)	2.51	(32.49)	(0.49)
	Br^{82}	0.0410	1.58	33.42	0.62
	I^{126}	0.0041	2.18	50.82	0.42
	I^{128}	0.0689	1.42	51.58	0.38
	Xe^{129}	0.0075	2.03	51.97	0.37
	I^{130}	0.318	0.76	52.24	0.24

Table XIII. (cont.)

He^4 Energy (MeV)	Isotope	Fractional chain yield	$(Z-Z_p)$[a]	Z_p	$(Z_p-0.4A)$
33.8	Br^{82}	0.0295	1.68	33.32	0.52
	I^{126}	0.0021	2.32	50.68	0.28
	I^{128}	0.0421	1.57	51.43	0.23
	Xe^{129}	0.0039	2.18	51.82	0.22
	I^{130}	0.251	0.88	52.12	0.12
28.0	Br^{82}	0.0192	1.80	33.20	0.40
	I^{126}	0.00071	2.53	50.47	0.07
	I^{128}	0.0204	1.78	51.22	0.02
	Xe^{129}	0.00181	2.34	51.66	0.06
	I^{130}	0.164	1.10	51.90	-0.10

[a] $(Z-Z_p)$ obtained from the Gaussian distribution of width constant c = 0.95.

REFERENCES

1. R. W. Spencer and G. P. Ford, Ann. Rev. Nuclear Sci. 2, 399 (1953).
2. I. Halpern, Ann. Rev. Nuclear Sci. 9, 245 (1959).
3. Earl K. Hyde, A Review of Nuclear Fission. Part I, Lawrence Radiation Laboratory Report UCRL-9036-Rev. April 1962 (unpublished).
4. Earl K. Hyde, A Review of Nuclear Fission. Part II, Lawrence Radiation Laboratory Report UCRL-9065, February 1960 (unpublished).
5. H. G. Thode and R. L. Graham, Can. J. Research A25, 1 (1947).
6. J. Macnarma, C. B. Collins, and H. G. Thode, Phys. Rev. 78, 129 (1950).
7. M. G. Inghram, R. J. Hayden, and D. C. Hess, Phys. Rev. 79, 271 (1950).
8. L. E. Glendenin, E. P. Steinberg, M. G. Inghram, and D. C. Hess, Phys. Rev. 84, 860 (1951).
9. D. R. Wiles, B. W. Smith, R. Horsley, and H. G. Thode, Can. J. Phys. 31, 419 (1953).
10. E. P. Steinberg, L. E. Glendenin, M. G. Inghram and D. C. Hess, Phys. Rev. 95, 867 (1954).
11. W. H. Fleming, R. H. Tomlinson, and H. G. Thode, Can. J. Phys. 32, 522 (1954).
12. R. K. Wanless and H. G. Thode, Can. J. Phys. 33, 541 (1955).
13. E. A. Melaika, M. J. Parker, J. A. Petruska, and R. H. Tomlinson, Can. J. Chem. 33, 830 (1955).
14. J. A. Petruska, E. A. Melaika, and R. H. Tomlinson, Can. J. Phys. 33, 640 (1955).
15. J. A. Petruska, H. G. Thode, and R. H. Tomlinson, Can. J. Phys. 33, 693 (1955).
16. T. J. Kennett and H. G. Thode, Phys. Rev. 103, 323 (1956).
17. E. P. Steinberg and L. E. Glendenin, in Proceedings of the Second United Nations International Conference on the Peaceful Uses of Atomic Energy, Geneva, 1955 (United Nations, New York, 1956), Vol 7, p.3.
18. A. T. Blades, W. H. Fleming, and H. G.Thode, Can. J. Chem. 34, 233 (1956).
19. R. N. Ivanov, V. K. Gorshkov, M. P. Anikina, G. M. Kukavadze, and B. V. Ershler, The Soviet J. At. Energy 3, 1436 (1957).

20. V. K. Gorshkov, R. N. Ivanov, G. M. Kukavadze, and I. R. Reformatsky, Soviet J. At. Energy 3, 729 (1957).

21. Yung Yee Chu, Charged-Paritcle-Induced Fission: A Mass Spectrometric Yield Study (Ph.D. Thesis), Lawrence Radiation Laboratory Report UCRL-8926, November 1959 (unpublished).

22. D. R. Bidinosti, D. E. Irish, and R. H. Tomlinson, Can. J. Chem. 39, 628 (1961).

23. H. Farrar, H. R. Fickel, and R. H. Tomlinson, Can. J. Phys. 40, 1017 (1962).

24. H. Farrar, and R. H. Tomlinson, Nuclear Phys. 34, 367 (1962).

25. S. Katcoff, Nucleonics 18, 201 (1960).

26. A. C. Wahl, R. L. Ferguson, D. R. Nethaway, D. E. Troutner, and K. Wolfsberg, Phys. Rev. 126, 1112 (1962).

27. A. O. Newton, Phys. Rev. 76, 628 (1949).

28. Bruce M. Foreman, Spallation and Fission in Thorium-232 and The Masses of The Heaviest Elements (Ph.D. Thesis), University of California Radiation Laboratory Report UCRL-8223, April 1958 (unpublished).

29. M. E. Davis, The Fission of Th^{232} Induced by Intermediate Energy Helium Ions (Ph. D. Thesis), Purdue University, January 1963 (unpublished).

30. L. E Glendenin, C. D. Coryell, and R. R. Edwards, in The National Nuclear Energy Series, (McGraw-Hill Book Company, Inc. New York, 1951). Vol. 9, Div. IV, p.489.

31. A. C. Pappas, M.I.T. Technical Report No. 63 (AECU-No.2806), September 1953 (unpublished).

32. A. C. Pappas, in Proceedings of the Second United Nations International Conference on the Peaceful Uses of Atomic Energy, (United Nations, New York, 1956) Vol. 7, pp.19 to 26.

33. W. E. Grummitt and G. W. Milton, (Chalk River Research Report CRC-694) (AECL-No. 453), May 1957 (unpublished).

34. A. C. Wahl, J. Inorg. Nucl. Chem. 6, 263 (1958).

35. C. D. Coryell, M. Kaplan, and R. D. Fink, Can. J. Chem. 39, 646 (1961).

36. H. M. Blann, Fission of Gold with 112-MeV C^{12} Ions: A Yield-Mass and Charge-Distribution Study (Ph.D. Thesis), Lawrence Radiation Laboratory Report UCRL-9190, May 1960 (unpublished).
37. J. Danon, J. Inorg. Chem. 5, 237 (1957).
38. S. E. Ritsema, Fission and Spallation Excitation Functions of U^{238} (M.S. Thesis) University of California Radiation Laboratory Report UCRL-3266, January 1956 (unpublished), p.7.
39. C. Williamson and J. P. Boujot, Tables of Range and Rate of Energy Loss of Charged Particles of Energy 0.5 to 150 MeV, Centre d' Etudes Nucleaires de Saclay, 1962 (unpublished).
40. Conductivity water courtesy of Dr. S. Thompson Group, Lawrence Radiation Laboratory, Berkeley.
41. F. W. Schuler, F. L. Steahly, and R. W. Stroughton, Paper 7.1 in Collected Papers, Production and Separation of U^{233}, ed. by L. I. Katzin, AEC Doc. TID-5223 (1952).
42. D. C. Hoffman and C. I. Browne, J. Inorg. Nucl. Chem. 2, 209 (1956).
43. P. C. Stevenson and W. E. Nervik, The Radiochemistry of The Rare Earths, Scandium, Yttrium, and Actinium, UCRL-5923, 1960 (unpublished).
44. Spiking solutions were prepared and cross-checked by Dr. Y. Y. Chu.
45. Advanced Vacuum Products Inc., 430 Fairfield Ave., Stamford, Conn.
46. Hoke Incorporated, Englewood, New Jersey (valves used were Nos. 415 and 413).
47. D. Alpert, Rev. Sci. Instr. 22, 536 (1951).
48. M. Pirani and J. Yarwood, Principles of Vacuum Engineering (Reinhold Published Corporation, New York 1961).
49. J. S. Allen, Phys. Rev. 55, 966 (1939).
50. M. Nakamura, M. C. Michel, and F. E. Vogelsberg, Mass Spectrometer Data Accumulator, in Lawrence Radiation Laboratory Chemistry Division Annual Report UCRL-10624 January 1963 (unpublished).
51. C. M. Stevens, Rev. Sci. Instr. 24, 148 (1953).
52. F. L. Reynolds, Vakuum-Tech. 8, 181 (1956).
53. J. H. Reynolds, Rev. Sci. Instr. 27, 928 (1956).

54. D. Strominger, J. M. Hollander, and G. T. Seaborg, Table of Isotopes, Rev. Mod. Phys. 30, 585-904 (1958).

55. H. M. Blann, Phys. Rev. 123, 1356 (1961).

56. B. D. Pate, J. S. Foster, and L. Yaffe, Can. J. Chem. 36, 1705 (1958).

57. W. J. Swiatecki (Lawrence Radiation Laboratory, Berkeley), private communication.

58. N. Souka and M. C. Michel, Mass Spectrometric Study of Mass and Charge Distribution in Fission of U^{233}, U^{235}, and U^{238}, Induced by Intermediate Energy Helium Ions, Lawrence Radiation Laboratory Report UCRL-10555, November 1962 (unpublished).

59. L. J. Colby, Jr., and J. W. Cobble, Phys. Rev. 121, 1410 (1961).

60. R. B. Leachman, in Proceedings of the Second United Nations International Conference on the Peaceful Uses of Atomic Energy (United Nations, Geneva, 1958), Vol. 15, p.229.

61. James A. Powers, Mass and Charge Distribution Studies in the Fission Of Np^{237} and Pu^{239} by Intermediate Energy Helium Ions (Ph.D. Thesis), Purdue University, January 1962 (unpublished).

62. W. E. Stein and S. L. Whetstone,Jr., Phys. Rev. 110, 476 (1958).

63. T. T. Sugihara, P. J. Drevinsky, E. J. Troianello, and J. M. Alexander, Phys. Rev. 108, 1264 (1957).

64. J. C. D. Milton and J. S. Fraser, Can. J. Phys. 40, 1626 (1962).

65. S. Cohen and W. J. Swiatecki, Ann. Phys. 19, 67 (1962).

66. S. L. Whetstone and R. B. Leachman, Bull. Am. Phys. Soc. 6, 376 (1961).

67. A. G. W. Cameron, Can. J. Phys. 35, 1021 (1957).

68. J. C. D. Milton, Fission Energy Tables and an Application to Nuclear Charge Division, Lawrence Radiation Laboratory Report UCRL-9883 Rev., January 1962 (unpublished).

69. A. E. S. Green, Phys. Rev. 95, 1006 (1954).

70. Eldon L. Haines, Mass-Energy Relations in the Fission of Highly Excited Heavy Nuclei (Ph.D. Thesis), Lawrence Radiation Laboratory Report UCRL-10342, June 1962 (unpublished).

71. R. H. Goeckermann and I. Perlman, Phys. Rev. 73, 1127 (1948).

72. Walter M. Gibson, Fission and Spallation Competition from the Intermediate Nuclei Americium-241 and Neptunium-235 (Ph.D. Thesis), Lawrence Radiation Laboratory Report UCRL-3493, November 1956 (unpublished).

73. J. M. Alexander and C. D. Coryell, Phys. Rev. 108, 1274 (1957).

74. Patrick del Marmol, Medium Energy Deuteron and Alpha Fission of U^{235} (Ph.D. Thesis), Massachusetts Institute of Technology, January 1959 (unpublished).

75. R. D. Present, Phys. Rev. 72, 7 (1947).

76. W. J. Swiatecki (Lawrence Radiation Laboratory, Berkeley), private communication to H. M. Blann.

77. R. Vandenbosch, T. D. Thomas, S. E. Vandenbosch, R. A. Glass, and G. T. Seaborg, Phys. Rev. 111, 1358 (1958).

78. J. S. Fraser and J. C. D. Milton, Phys. Rev. 93, 818 (1954).

79. S. L. Whetstone, Jr., Phys. Rev. 114, 581 (1959).

80. J. Terrell, Phys. Rev. 127, 880 (1962).

81. A. T. Blades and H. G. Thode, Z. Naturforsch. 10a, 838 (1955).

82. Willaim F. Biller, The Characteristics of Bismuth Fission Induced by 340-MeV Protons (Ph.D. Thesis), University of California Radiation Laboratory Report UCRL-2067, March 1953 (unpublished).

83. H. G. Hicks and R. S. Gilbert, Phys. Rev. 100, 1286 (1955).

84. Sylvia Mae Bailey, Independent Yields of Isomeric Pairs in Nuclear Reactions (Ph.D. Thesis) Lawrence Radiation Laboratory Report UCRL-8710, April 1959 (unpublished).

85. H. B. Levy and D. R. Nethaway, Bivariate Normal Distribution of Charge and Mass in Symmetric Fission as Applied to the Fission of Au^{197} with 112-MeV C^{12} Ions, Lawrence Radiation Laboratory Report UCRL-6948, June 1962 (unpublished).